NASA Technical Paper 1366

Fluctuating Loads Measured on an Over-the-Wing Supersonic Jet Model

Conrad M. Willis

JANUARY 1979

NASA

NASA Technical Paper 1366

Fluctuating Loads Measured on an Over-the-Wing Supersonic Jet Model

Conrad M. Willis
Langley Research Center
Hampton, Virginia

National Aeronautics
and Space Administration

**Scientific and Technical
Information Office**

1979

SUMMARY

A test was conducted to measure fluctuating pressure loads on the wing and flap of an over-the-wing supersonic jet model. The model was tested statically and at a Mach number of 0.1 in a small free jet to simulate forward speed. Test parameters were impingement angle, nozzle height, and flap deflection. Load levels as high as 170 dB were measured at the center of the impingement region during static tests. Forward speed reduced the loading about 1 dB. Load level increased with increasing impingement angle and decreasing nozzle height above the wing. The effect of flap deflection was small. When scaled to full-size aircraft conditions, the maximum amplitude of the one-third-octave fluctuating pressure spectra was about 154 dB at about 160 Hz. Maximum load level occurred near the intersection of the nozzle center line with the impinged surface. Downstream of the maximum the fluctuating pressure is inversely proportional to the distance downstream of the nozzle.

INTRODUCTION

Over-the-wing (OTW) mounting of jet engines is one of the concepts that has been examined by the NASA supersonic cruise aircraft research (SCAR) program to provide a technology base for future aircraft. Some of the possible advantages of the OTW configuration are Coanda lift augmentation for low-speed flight (refs. 1 and 2), a decrease in subsonic drag (ref. 3), and a reduction of ground noise (refs. 4 and 5). One potential disadvantage introduced by OTW engines is the high fluctuating pressure loading imposed on wing and fuselage surfaces lying within the jet impingement region (refs. 6 and 7). Since these loads are higher than the turbulent boundary-layer loading imposed on the adjacent surfaces, the use of OTW engines will probably require some structural design modification for the impinged areas to attain acceptable fatigue life and cabin noise levels. Use of model data to define these loads will permit inclusion of the appropriate structural properties in the early design stages of the aircraft.

Fluctuating pressure loads with OTW engines having subsonic nozzles have been extensively studied. (See refs. 8 to 10.) Some experiments have been performed in supersonic flow (refs. 4 and 11), but the results are less complete than those for subsonic nozzles. The present investigation was undertaken to provide better definition of the fluctuating pressure loading that would occur with one of the nozzle configurations being considered for OTW use on a SCAR configuration.

The present paper reports the spatial and spectral distribution of fluctuating pressure loads within the impingement region for a simulated supersonic jet engine configuration. The model was a two-dimensional wing with a 3.15-cm-diameter plug-nozzle cold-air jet mounted above the upper surface. The nozzle Mach number was 1.4. Testing was conducted in two anechoic rooms; in one the model was mounted in a free jet exhausting into

an anechoic chamber; in the other the model was tested statically. Test variables were engine height above the wing, chordwise location of the engine, jet impingement angle, flap deflection, and airspeed. Results are presented to show the effects of the various test parameters on the overall level and the power spectral density of the fluctuating pressure loads. Cross-correlation and coherence data are presented for a few measurement locations and one load spectrum is extrapolated to full-scale conditions.

SYMBOLS AND ABBREVIATIONS

c	wing chord, 51 cm
D	jet exit diameter (see fig. 1(d)), cm
dB	decibel, $20 \log \frac{p}{p_r}$
EBF	externally blown flap
FPL	fluctuating pressure level, intensity within a particular frequency band, dB
f	frequency, Hz
h	nozzle height, measured from lower edge of exit to wing upper surface (see fig. 1(d)), cm
M_j	jet Mach number
M_∞	free-stream Mach number of free jet
OAFPL	overall fluctuating pressure level, dB
OTW	over-the-wing mounting of engines
p	root-mean-square value of fluctuating pressure, Pa
p_r	reference pressure, 20 μPa
PSD	power spectral density, fluctuating pressure level for 1 Hz bandwidth, dB
q	dynamic pressure of jet, $\rho V^2/2$, Pa
T	static temperature at jet exit, K
USB	upper surface blowing
V	jet velocity at exit, m/s

x distance aft of jet exit, cm

y distance outboard of jet center line, cm

δ flap deflection, deg

θ jet impingement angle, measured from nozzle center line to wing upper surface, deg

ρ density, $kg\text{-}s^2/m^4$

ϕ cross-spectral density phase angle, deg

Subscripts:

fs full scale

m model

APPARATUS AND PROCEDURE

Test Facilities

Testing was carried out in two large (about 500 m^3 volume) anechoic rooms; one was located in the Langley anechoic noise facility and the other, in the Langley aircraft noise reduction laboratory. The test facilities are shown schematically in figure 1(a). One facility was used for static tests and the test program was completed in a second facility which could be used for forward-speed tests. Unheated compressed dry air was supplied to the supersonic jet nozzle. Air pressure was adjusted by a manual valve in the supply line. The forward-speed tests were conducted in a 20-cm-diameter free jet issuing from the anechoic room wall. The free jet was operated at a Mach number of 0.1.

Models

Two models, having equal size, were constructed because of differences in mounting fixtures available for the two test facilities. A sketch of model 1, the static test model, is presented in figure 1(b). The model consisted of a wing, plug nozzle, and fuselage section. The wing is a two-dimensional airfoil having a 51-cm chord. This chord represents a model scale of about 1/70 referenced to the SCAT 15F design used as the baseline configuration for the SCAR program. Wing span for the model is 46 cm. The wing was translated and rotated on the mounting fixture to vary nozzle height h above the wing, and jet impingement angle θ. The simulated plug nozzle engine is mounted separately on a telescoping air supply pipe that allows adjustment of the chordwise location of the nozzle. Interchangeable wing trailing-edge sections were used to vary the flap deflection angle δ. A 6-cm-diameter rounded-nose cylindrical body extending fore and aft of the wing represents the fuselage. The engine center line was located about 1.5 nozzle diameters outboard of the fuselage sidewall. Model 2, the forward-speed effects model, is shown in

figure 1(c). Model 2 is the same size as model 1 but differs in having a pylon that attaches the engine to the wing. Impingement angle and nozzle location are varied by changing the middle sections of the nacelle.

Figure 1(d) presents some of the details of the plug nozzle design. Nozzle Mach number is 1.42, jet exit diameter D is 3.15 cm, and annular exit area is 2.3 cm^2. This nozzle configuration is one of the designs considered for OTW use by the SCAR program systems studies. The disk supporting the plug also serves as a flow straightener. Open area for the disk was about twice the throat area. A thermocouple and a static-pressure measurement port located between the plug and flow straightener provided measurements of nozzle flow conditions.

A photograph of model 2 is presented as figure 2. The engine is near the center line of the free jet nozzle. The nose of the fuselage extends inside the nozzle.

Instrumentation

Strain-gage-type fluctuating pressure transducers having a diameter of 0.3 cm and a natural frequency of about 70 kHz were mounted flush with the surface of the model at the 11 locations as indicated in table I. Table II lists the chordwise distance from the fixed transducer locations to the various nozzle locations examined in this test.

Transducer outputs were amplified and high pass filtered to remove the direct-current component before recording. The data were recorded on a 14-channel magnetic tape recorder operated at a tape speed of 300 cm/s. Nozzle air supply pressure and ambient pressure were read from dial gages and the desired ratio of supply to ambient pressure was obtained by adjusting a valve in the air supply line. The pressure transducers were calibrated at the beginning and end of the test by applying an acoustic input to determine gage sensitivity and applying a common white-noise voltage input to determine interchannel phase angles for the amplifier-recorder system.

Data accuracy was not estimated; however, repeated measurements at the same test condition agreed within 0.3 dB. Therefore, small differences in OAFPL between sets of measurements from a given transducer were sometimes considered sufficient to indicate trends because most of the possible error sources (for example, vibration sensitivity and calibration error) were about the same level for both sets of data.

Test Procedure

Testing was conducted in two anechoic chambers. After placing the engine at the desired location, the air supply valve was opened until the nozzle was operating at the 3.22 design pressure ratio. The free jet flow was then adjusted to the desired Mach number by changing the speed of a centrifugal blower and the data from the fluctuating pressure transducers

were recorded on magnetic tape. The test variables and their ranges were as follows:

Jet impingement angle, deg	0 to 12
Jet exit location, percent chord	10 to 87
Nozzle height above wing, diameters	0.3 to 1.5
Flap deflection, deg	5 to 45
Free-jet Mach number	0 or 0.1

The model was mounted at an angle of attack of about 4.5° to the wind-tunnel flow. The temperatures of the air supplies for the supersonic jet and free jet nozzles varied from 0° to 30° C. Ambient pressure in the test chambers was between 100.6 and 103.4 kPa and the relative humidity was between 35 and 80 percent.

RESULTS AND DISCUSSION

The fluctuating pressure data were processed and analyzed to obtain overall levels and power spectra. The data were then compared to determine the effects of the various test parameters. Cross-correlation and coherence functions were also determined for a few test conditions.

Overall Levels of Loads

Comparison of data from the two models.- Figure 3 presents comparisons of the data from the two tests to show that any differences in the models, air supply, or test facility were not large enough to have a substantial effect on the data. The differences were found to be quite small; therefore, the model used will not be identified in subsequent figures.

Chordwise nozzle location.- Variation in overall fluctuating pressure level (OAFPL) with chordwise location of the nozzle for two jet center-line transducer locations is presented in figure 4(a). The highest level, about 170 dB, was measured for a nozzle exit location at 50 percent of the wing chord. With the 50-percent-chord nozzle location, the nozzle center line intersects the wing surface at 81 percent chord or a little aft of transducer H, which is located at 75 percent chord. Thus, the peak load appears to occur near the intersection of the nozzle center line with the impinged surface and the loading decreases with distance from the nozzle. The nozzle center line does not intersect the wing for the two aft nozzle locations (65 and 87 percent chord) and the flow turning is probably incomplete. Overall fluctuating pressure level along the nozzle center line as a function of distance from the nozzle is presented in figure 4(b). For measurement locations downstream of the maximum load, the level appears to fall off at a rate equivalent to p being inversely proportional to x^2 as reported for subsonic impingement in reference 12. With $h/D = 0.3$ and $\theta = 9^\circ$, the jet center line intersects the wing upper surface at about $x/D = 5$; this is the location of the peak load for measurements forward of the knee of the flap. Aft of the flap knee, the peak load location is influenced by the flow turning but the peak amplitude and the rate of decay appear to be unchanged. Figure 4(c) presents spanwise load profiles for various

distances forward and aft of the nozzle. The load level decreases rapidly with lateral distance from the nozzle center line.

Figure 5 presents the overall fluctuating pressure level (OAFPL) isobars for the fluctuating pressure loading on the wing surface adjacent to the nozzle. This figure is a cross plot of faired data. The load level has a steep gradient spanwise and a more gradual change chordwise. The region having a loading equal to or greater than 140 dB is about 10 nozzle diameters wide and extends from near the nozzle to more than 10 diameters to the rear. Flight loadings as high as 140 dB have been measured on areas well outside the impingement region. (See ref. 10.) Therefore, the area enclosed by the 140-dB isobar is taken as an approximation of the area that may require additional structural design attention because of the use of an OTW configuration. Outside the 140-dB isobar, other design constraints such as the turbulent boundary loading would probably dictate the structural requirements.

Airspeed.- The effect of forward velocity or airspeed on the overall fluctuating pressure levels is presented in figure 6. In figure 6(a) the loading along the nozzle center line for a free-stream Mach number of 0.1 is compared with the static loading and in figure 6(b) a spanwise comparison is presented. There appears to be a small reduction of about 1 dB from the static level throughout the impinged region forward of the knee of the flap. The outboard measurement location ($y/D = 4.8$) in figure 6(b) is outside the impingement region, and within but near the edge of the free jet flow. The loading inboard of the engine ($y/D = -1.2$) is about 2 dB higher than the corresponding outboard measurement, probably because of interference from the fuselage sidewall.

Flap deflection.- Figure 7 presents the variation in flap loading with flap deflection angle for two nozzle locations. Flap loading was nearly constant for flap deflections of 5° to 45°. The nozzle center line at the aft location, 56 percent chord corresponding to $x/D = 6$, intersects the wing surface just forward of the flap and most of the jet flow is probably attached to the surface before encountering the knee of the flap.

Impingement angle.- Overall fluctuating pressure levels along the nozzle center line for jet impingement angles of 0° to 12° are presented in figure 8. At the higher impingement angles the OAFPL maximum increases and the location of the maximum moves closer to the nozzle exit. The change in OAFPL with impingement angle appears to be greatest about three nozzle diameters downstream of the exit. The impingement angle for most upper surface blowing (USB) applications will probably lie in the 5° to 10° range that has been used in subsonic tests (ref. 8) with the smallest angle that will provide satisfactory turning for the particular configuration being selected. The nozzle angle will probably be adjustable in flight and will be decreased when the flaps are retracted.

Nozzle height.- Over-the-wing (OTW) supersonic nozzle designs may mount the engines on pylons that elevate the nozzle above the wing surface to reduce the jet impingement in the cruise condition. Figure 9 presents fluctuating pressure loading along the nozzle center line for four nozzle heights. For nozzle center-line locations three to nine diameters aft of the nozzle exit, where most of the measurements were made, the load level appears to decrease

about 10 dB per diameter of elevation. However, elevation of the engine would probably be limited to values of $h/D < 1$ by weight of the support pylon and difficulty in obtaining attached flow. The load reductions with nozzle elevation for 0^{o} and 9^{o} impingement angles were about equal. There appears to be a decrease in the effect of nozzle height for distances greater than $x/D = 10$ aft of the nozzle.

Spectral Distribution of Loads

Variation with location.- Fluctuating pressure spectra for 10 locations at $M_{\infty} = 0$ are presented in figure 10. Spectra for nozzle center-line locations (O, H, P, and N) are relatively flat from 200 Hz to about 8000 Hz and then decrease at a rate of about 8 dB per octave. Spectra for the two fuselage sidewall transducer locations, A and B, started to fall off at a higher frequency of about 30 000 Hz. However, for frequencies up to about 10 000 Hz the spectrum for fuselage location B is similar to that for the adjacent location G on the wing surface. Spectra for off-center-line locations tend to have sharper peaks with increasing distance from the center line, for example, locations I and L which lie, respectively, inside and outside the impingement region. The sharp peak in the spectrum for location L may be part of the shock structure. Comparison of the spectra for locations I and G indicates that the presence of the fuselage had little effect on the wing loads except for the slightly higher level adjacent to the fuselage that was previously noted in figure 6(b).

Airspeed.- Spectra for two values of tunnel Mach number are compared in figure 11(a). A Strouhal number frequency scale is shown for reference at the top of the figure. A free-stream Mach number of 0.1 reduced the fluctuating pressure level 1 to 3 dB below the $M_{\infty} = 0$ level over most of the frequency range up to 6000 Hz. This reduction amounted to an overall decrease of about 1 dB. Aft of the knee of the flap, airspeed had little effect on fluctuating pressure levels as shown by the nearly identical spectra for $M_{\infty} = 0$ and $M_{\infty} = 0.1$ presented in figure 11(b).

Impingement angle.- Spectra for impingement angles of 9^{o} and 12^{o} are compared in figure 12. Spectra shapes are similar at frequencies above 1 kHz and peaks occur at the same frequencies. The 3^{o} increase in impingement angle produced a 2-dB increase in OAFPL. The sharp peak at 8 kHz becomes less pronounced at greater distances from the nozzle.

Cross correlation and coherence.- Cross-correlation coefficients and coherence functions for two nozzle center-line locations separated by a distance of about 1 nozzle diameter are presented in figure 13. Spectra for the two locations, shown at the top of the figure, were similar in both shape and level. The cross-correlation coefficients are low, about 0.4 for $M_{\infty} = 0$ (fig. 13(a)) and 0.3 for $M_{\infty} = 0.1$ (fig. 13(b)). The peak coefficient occurs at a delay time of about 0.1 msec. Dividing the transducer separation distance by this delay time gives a convection velocity of about 300 m/s or about three-fourths of the nozzle exit velocity, for the the rate of propagation of a flow disturbance between transducers. The coherence function was also generally low, less than 0.5, except for a few narrow bands. For the sample shown, the band of high coherence is about 3 to 6 kHz and roughly corresponds to the

range of the highest peaks in the spectra for the pair of locations being examined. Cross-correlation coefficients and coherence functions were both lowered by forward velocity but the convection velocity remained about the same.

Phase angle.- The cross-spectral-density phase angles for two sets of transducer locations are presented in figure 14. The free-jet-off ($M_\infty = 0$) phase angle plots are nearly straight lines and indicate that the convection velocity is about the same over the frequency range. The convection velocity, obtained by dividing the transducer separation distance by the quantity $\phi/360f$, is about 290 m/s for the H × M transducer pair at the static condition. This value agrees within 3 percent with the convection velocity obtained from the cross-correlation coefficient of the same set of data presented in the previous figure. Above a frequency of about 10 kHz, an airspeed of 41 m/s ($M_\infty = 0.1$) had little or no effect on the convection velocity. At lower frequencies, forward velocity reduced the convection velocity by as much as 20 percent. Convection velocity also decreased with distance from the nozzle. The data shown for aft transducer pair M × N, which were separated by the knee of the flap, indicate a convection velocity about 30 percent lower than that for H × M.

Comparisons With Other Configurations

Pressure coefficients.- Figure 15 compares the pressure coefficients for the small-scale supersonic jet used in the present test with the data presented in reference 13 for subsonic jets. The range indicated for the present test is the range in loading shown in figure 5 along the nozzle center line for x/D values of 2 to 10 with $h/D = 0.3$ and $\theta = 9^o$. The maximum coefficient value for the supersonic nozzle was 0.06, about one-half the maximum value for the subsonic configurations shown in figure 15.

Full-scale spectra.- A one-third-octave spectrum scaled from model data to a full-size aircraft is presented in figure 16. The data were scaled by the nondimensional factors used in references 9 and 14, namely, $f\frac{D}{V}$ or Strouhal number for the frequency scale and (PSD) (V/q^2D) for the magnitude. The basic forms of the equations used are

$$f_{fs} = \left(f\frac{D}{V}\right)_m \left(\frac{V}{D}\right)_{fs}$$

and

$$(PSD)_{fs} = (PSD)_m \left(\frac{D_{fs}}{D_m}\right)\left(\frac{q_{fs}^2 V_m}{q_m^2 V_{fs}}\right)$$

where the subscripts fs and m refer to full-scale and model quantities. For constant percentage bandwidth spectra such as one-third octave bands, the (D_{fs}/D_m) term in the PSD equation disappears and the magnitude of the spectra becomes independent of model size (ref. 15) and

$$(\text{one-third-octave FPL})_{fs} = (\text{one-third-octave FPL})_m \left(\frac{q_{fs}^2 V_m}{q_m^2 V_{fs}} \right)$$

Since specifications and jet conditions for real engines are commonly given in terms of velocity and temperature, the substitution of $q = k \frac{V^2}{T}$ was made, where T is the gas temperature and the constant k was assumed to be equal for the exhaust gases from the model and full-scale engines. The final form of the equation for the magnitude of the scaled spectrum then becomes

$$(\text{one-third-octave FPL})_{fs} = (\text{one-third-octave FPL})_m \left(\frac{V_{fs}^3 T_m^2}{V_m^3 T_{fs}^2} \right)$$

The model spectrum selected as typical for scaling was obtained from a nozzle center-line transducer (location H) at a distance $x/D = 8.9$ aft of the nozzle at static conditions, $M_\infty = 0.0$. Measured OAFPL was 167 dB. Model nozzle diameter was 3.15 cm and the jet exhaust air had a velocity of 415 m/s, and a temperature of 210 K. The corresponding conditions for the full-scale aircraft, selected with the intention of representing some future supersonic aircraft in a landing-approach mode, are a nozzle diameter of 2.1 meters and jet efflux temperature and velocity of 600 K and 700 m/s. For the conditions selected to represent full-scale conditions, the spectrum appears to have a peak of about 154 dB near a one-third-octave center frequency of 250 Hz and most of the energy lies between 12 and 1250 Hz. Loads of this magnitude should receive some design attention.

CONCLUSIONS

Fluctuating pressure loads in the jet impingement region have been measured for an over-the-wing configuration. The model jet was a 3-cm-diameter cold-air Mach 1.4 plug nozzle. Data were obtained for a range of engine locations and impingement angles. The results have led to the following conclusions:

1. Fluctuating pressure loads at the center of the impingement region are high, up to 170 dB.

2. Forward speed provides a slight reduction in loading but the levels are still high enough to indicate the need for design consideration in the impingement region.

3. Maximum load level occurred near the intersection of the nozzle center line with the impinged surface. Downstream of the maximum the fluctuating pressure is inversely proportional to the distance downstream of the nozzle as has been reported for subsonic jet impingement.

4. Nozzle height and impingement angle had a significant effect on model loads; the effect of flap deflection was smaller.

5. The maximum observed value for the fluctuating pressure coefficient along the nozzle center line of the Mach 1.4 supersonic nozzle was 0.06 which is about one-half the magnitude of coefficients reported for subsonic nozzles.

Langley Research Center
National Aeronautics and Space Administration
Hampton, VA 23665
November 16, 1978

REPERENCES

1. Shivers, James P.; McLemore, H. Clyde; and Coe, Paul L., Jr.: Low-Speed Wind-Tunnel Investigation of a Large-Scale Advanced Arrow-Wing Supersonic Transport Configuration With Engines Mounted Above Wing for Upper-Surface Blowing. NASA TN D-8350, 1976.

2. Coe, Paul L., Jr.; and Graham, A. B.: Results of Recent NASA Research on Low-Speed Aerodynamic Characteristics of Supersonic Cruise Aircraft. Proceedings of the SCAR Conference - Part 1, NASA CP-001, [1977], pp. 123-136.

3. Mercer, Charles E.; and Carson, George T., Jr.: Upper Surface Nacelle Influence on SCAR Aerodynamic Characteristics at Transonic Speeds. Proceedings of the SCAR Conference - Part 1, NASA CP-001, [1977], pp. 137-154.

4. Guinn, Wiley A.; Balena, Frank J.; Clark, Lorenzo R.; and Willis, Conrad M.: Reduction of Supersonic Jet Noise by Over-the-Wing Engine Installation. NASA CR-132619, 1975.

5. Reshotko, Meyer; Goodykoontz, Jack H.; and Dorsch, Robert G.: Engine-Over-the-Wing Noise Research. AIAA Paper 73-631, July 1973.

6. Goetz, Robert C.: Loads Technology for Supersonic Cruise Aircraft. Proceedings of the SCAR Conference - Part 2, NASA CP-001, [1977], pp. 685-706.

7. Guinn, Wiley A.; Balena, Frank J.; and Soovere, Jaak: Sonic Environment of Aircraft Structure Immersed in a Supersonic Jet Flow Stream. NASA CR-144996, 1976.

8. Mixson, John S.; Shoenster, James A.; and Willis, Conrad M.: Fluctuating Pressures on Aircraft Wing and Flap Surfaces Associated With Powered-Lift Systems. AIAA Paper 75-472, Mar. 1975.

9. Haviland, J. K.; and Herling, W. W.: Modelling Techniques for Jet Impingement. AIAA Paper 77-591, June 1977.

10. Butzel, L. M.; Jacobs, L. D.; O'Keefe, J. V.; and Sussman, M. B.: Cabin Noise Behavior of a USB STOL Transport. AIAA Paper 77-1365, Oct. 1977.

11. Heller, Hanno H.; and Clemente, Anthony R.: Fluctuating Surface-Pressure Characteristics on Slender Cones in Subsonic, Supersonic, and Hypersonic Mach-Number Flow. NASA CR-2449, 1974.

12. Westley, R.; Woolley, J. H.; and Brosseau, P.: Surface Pressure Fluctuations From Jet Impingement on an Inclined Flat Plate. Symposium on Acoustic Fatigue, AGARD-CP-113, May 1973, pp. 4-1 - 4-17.

13. Lansing, Donald L.; Mixson, John S.; Brown, Thomas J.; and Drischler, Joseph A.: Externally Blown Flap Dynamic Loads. STOL Technology, NASA SP-320, 1972, pp. 131-142.

14. Willis, Conrad M.; Schoenster, James A.; and Mixson, John S.: Acoustic Loads on Upper-Surface-Blown Powered-Lift Systems. AIAA Paper 77-1363, Oct. 1977.

15. Bies, David A.; and Franken, Peter A.: Notes on Scaling Jet and Rocket Noise. J. Acoust. Soc. America, vol. 33, no. 9, Sept. 1961, pp. 1171-1173.

TABLE I.- TRANSDUCER LOCATION

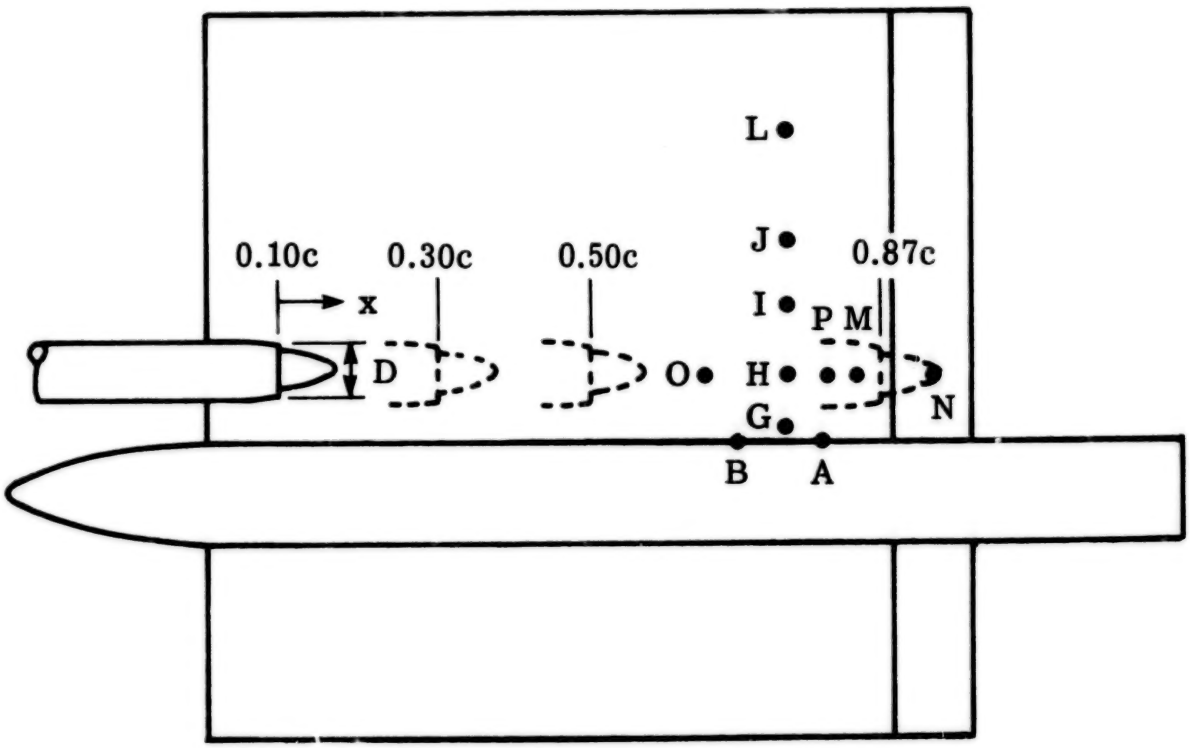

Transducer	Transducer location		Site on model
	Percent c	y/D	
O	65	0	Wing
G	75	-1.21	
H	75	0	
I	75	1.21	
J	75	2.42	
L	75	4.84	
M	84	0	
P	81	0	
N	95	0	Flap
A	80	-1.57	Fuselage
B	70	-1.57	

TABLE II.- DISTANCE FROM NOZZLE TO TRANSDUCER, x/D

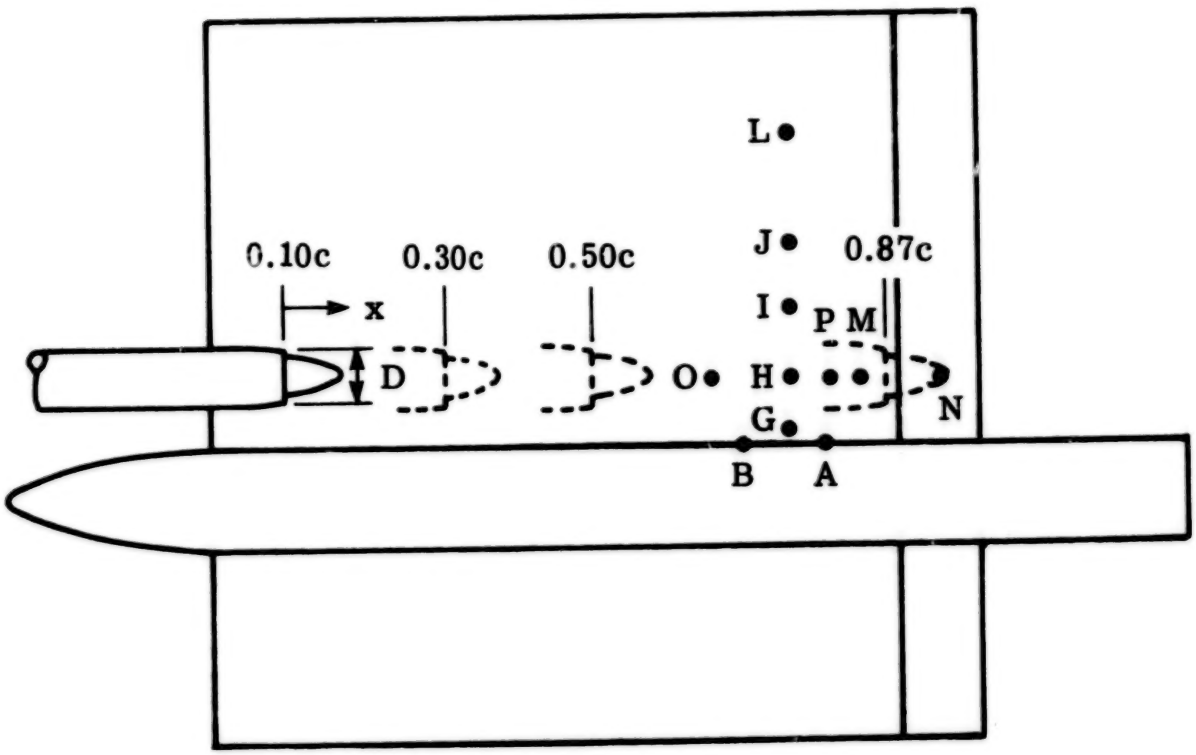

Nozzle location, percent c	Distance to transducer for -										
	Wing locations								Flap location	Fuselage locations	
	O	G	H	I	J	L	M	P	N	A	B
10		10.5	10.5	10.5	10.5	10.5	11.9		13.7		
20		8.9	8.9	8.9	8.9	8.9			12.1		
23							9.8				
25			8.1								
30		7.3	7.3	7.3	7.3	7.3			10.5		
40		5.6	5.6	5.6	5.6	5.6			8.9		
50	2.4	4.0	4.0	4.0	4.0	4.0	5.5	4.9	7.3	4.8	3.2
56		3.1	3.1				4.5		6.3		
65	0	1.6	1.6				3.1	2.5	4.8		
87		-2.0	-2.0						1.2		

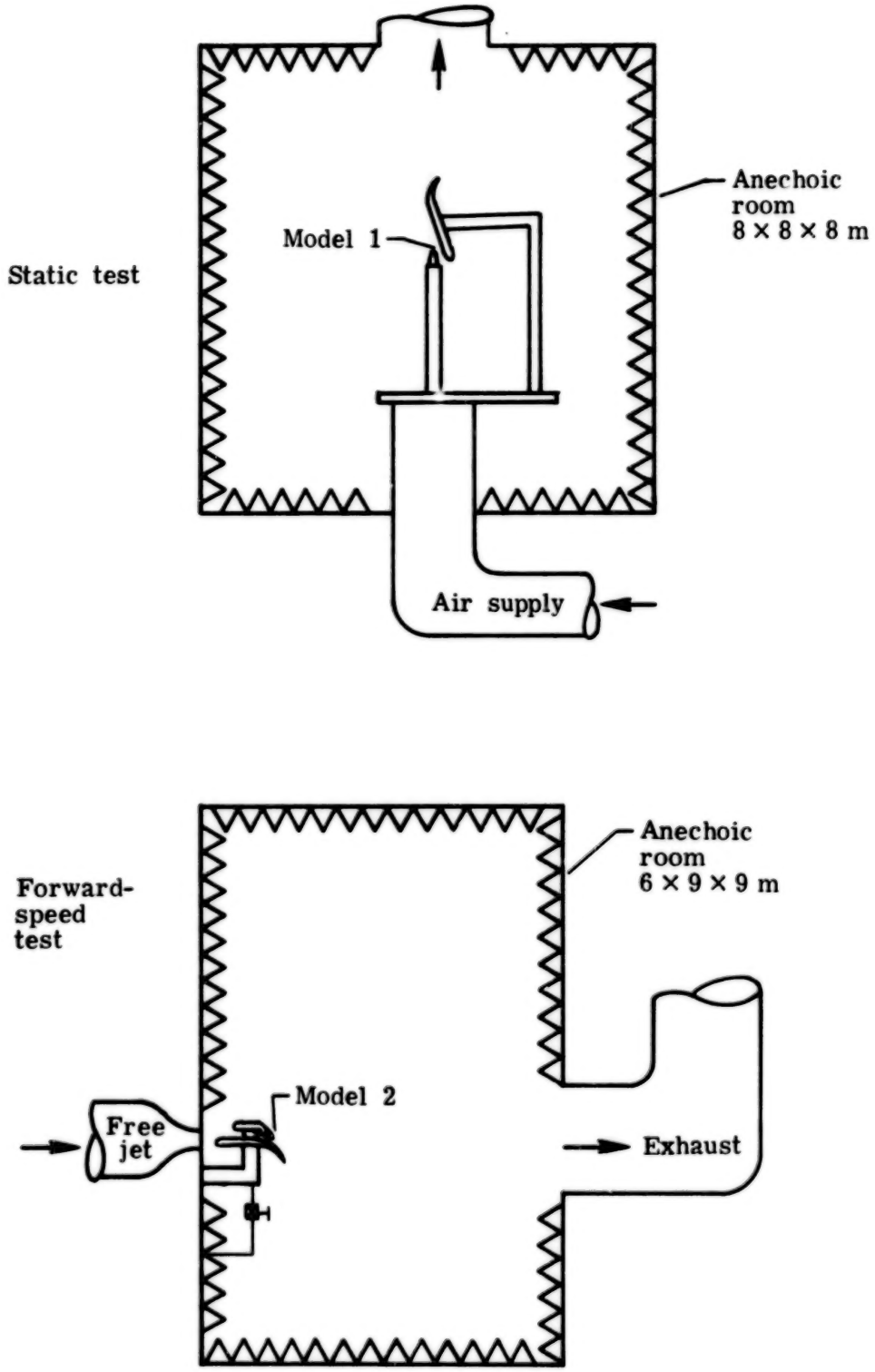

(a) Schematic of test facilities.

Figure 1.- Over-the-wing models and test apparatus.

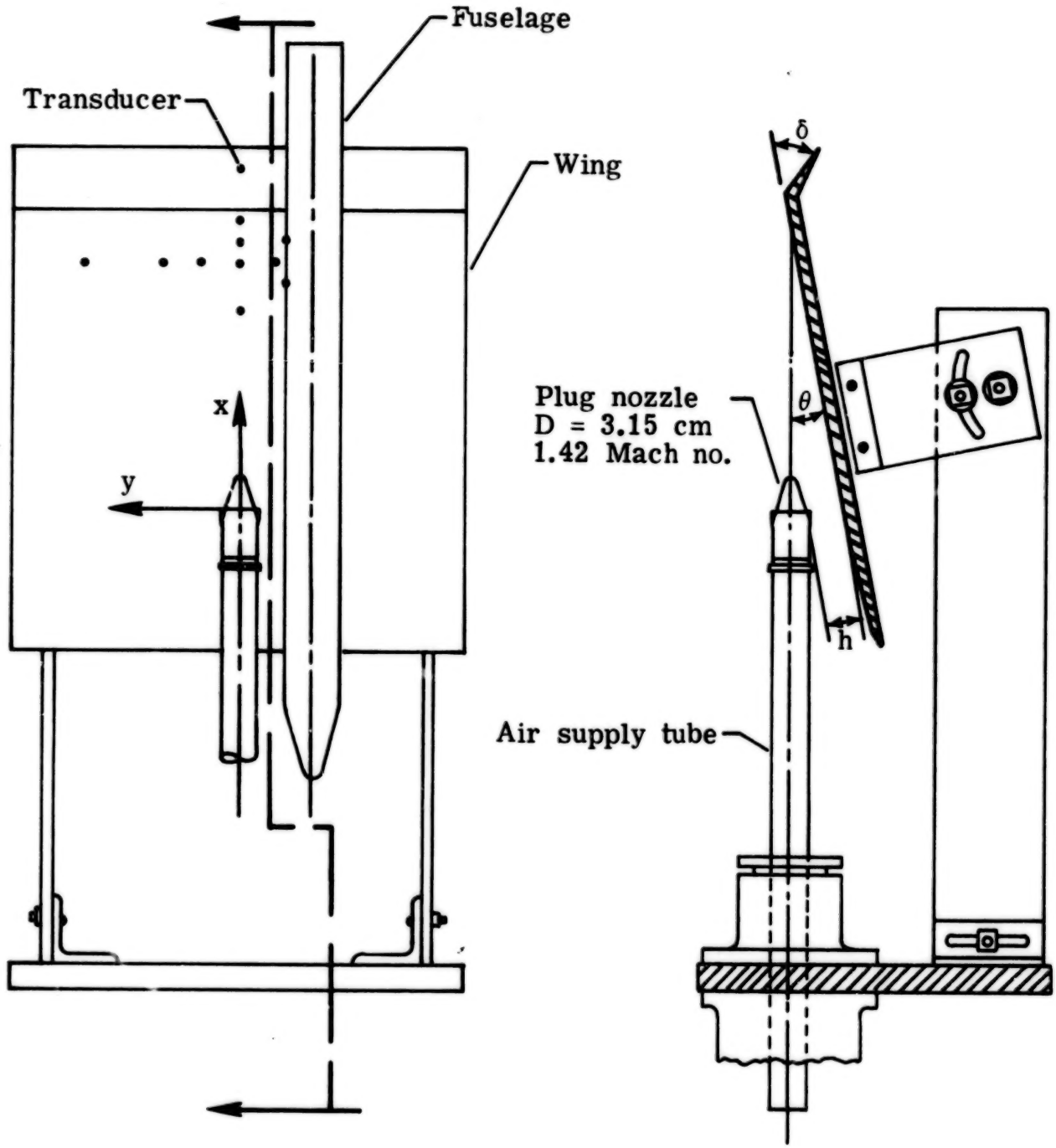

(b) Model 1.

Figure 1.- Continued.

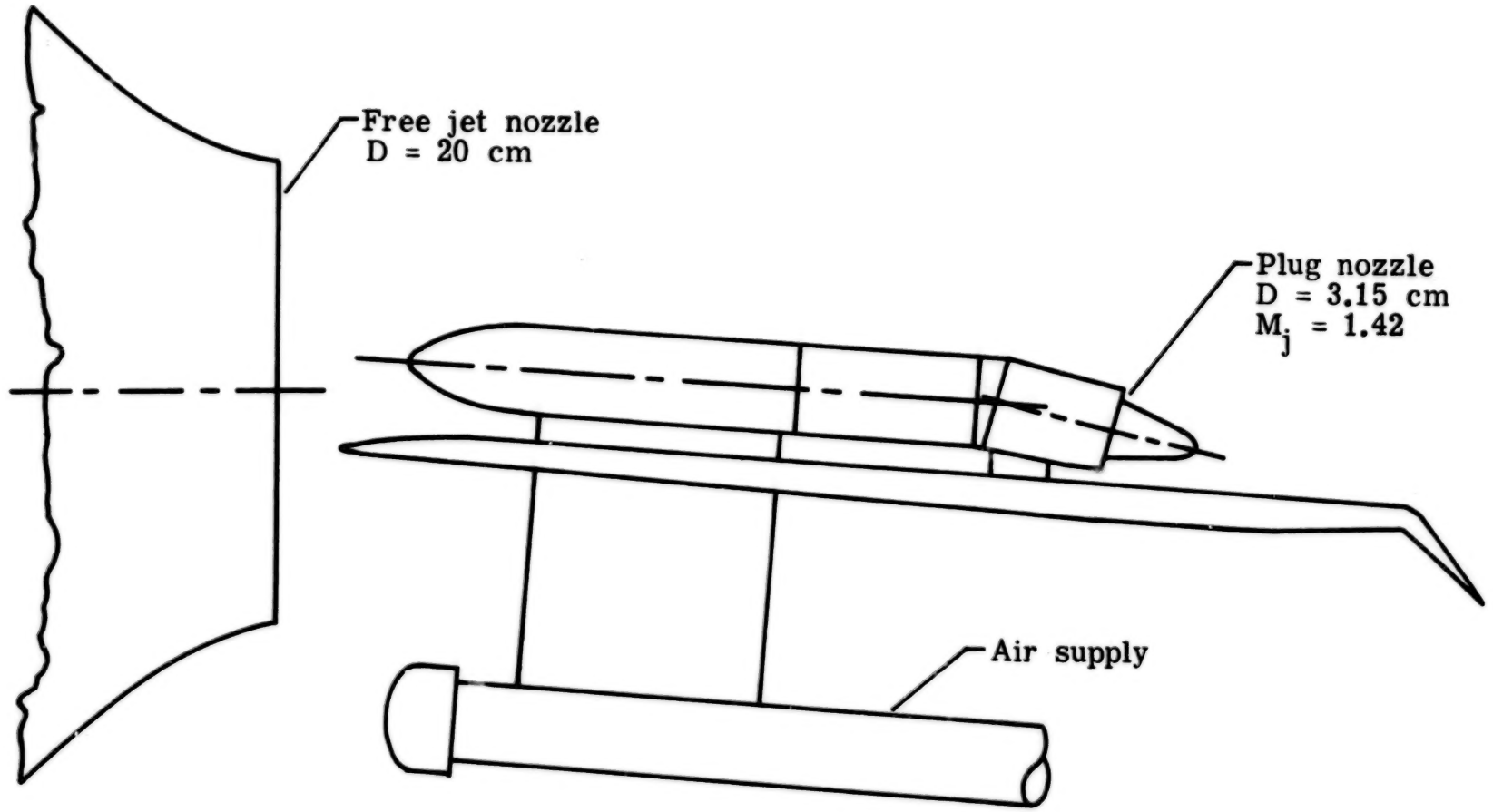

(c) Model 2.

Figure 1.- Continued.

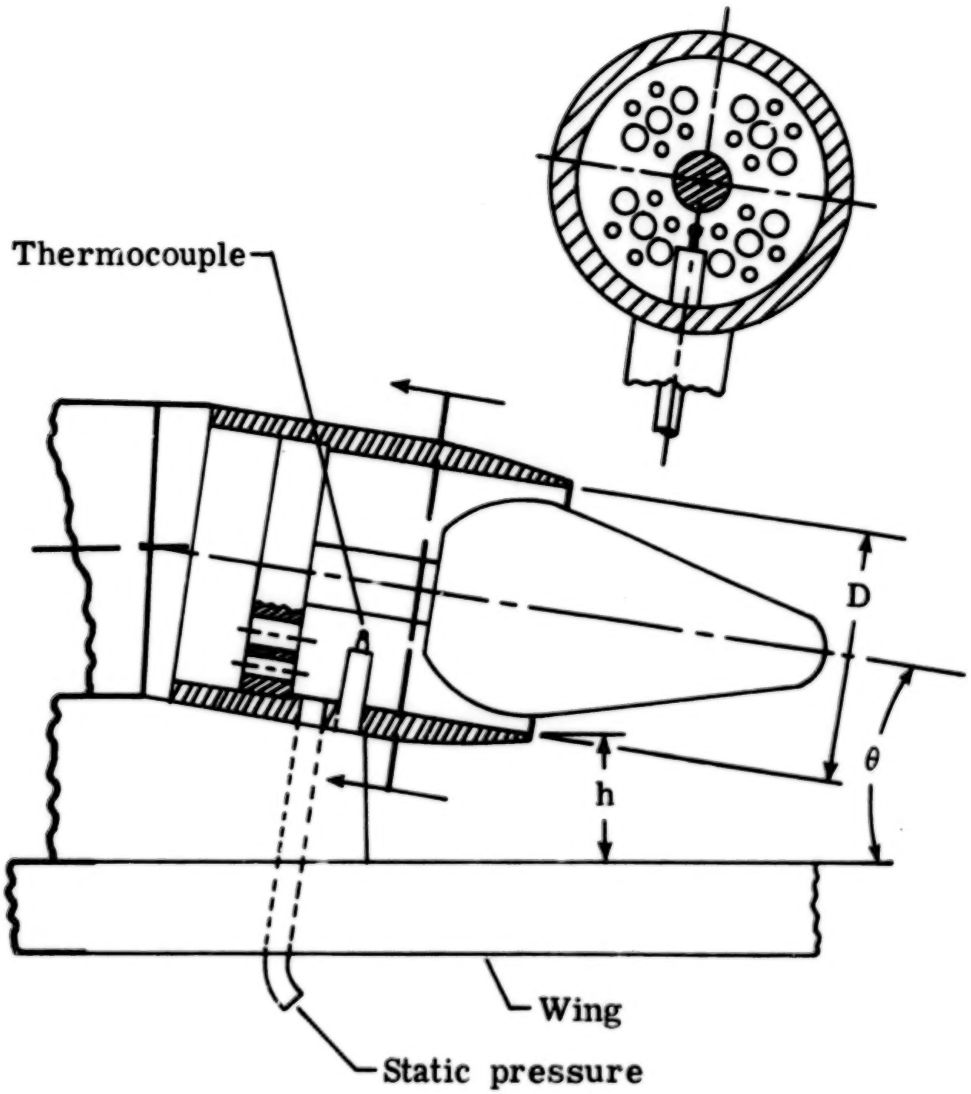

(d) Nozzle details.

Figure 1.- Concluded.

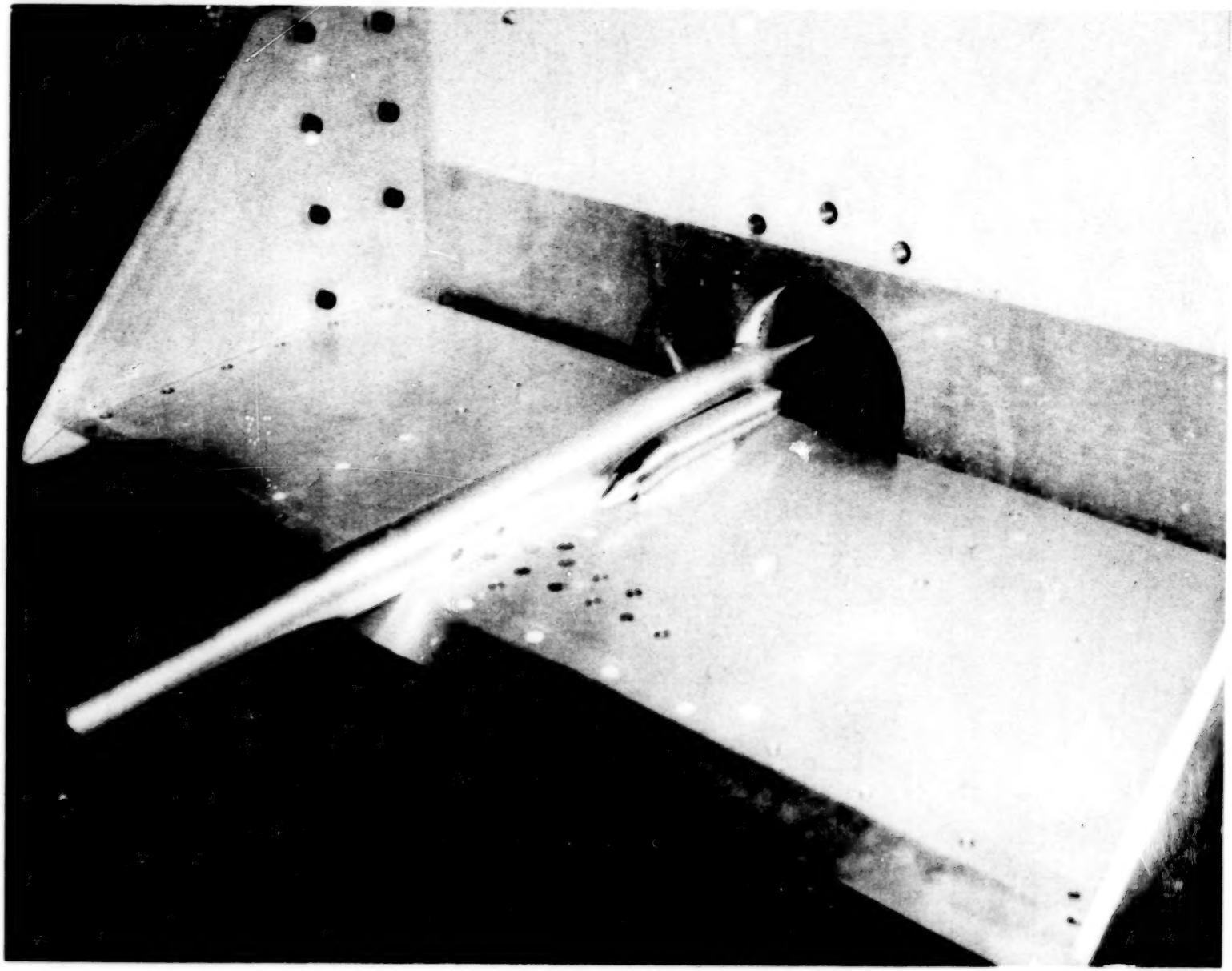

L-76-7279

Figure 2.- Photograph of model 2.

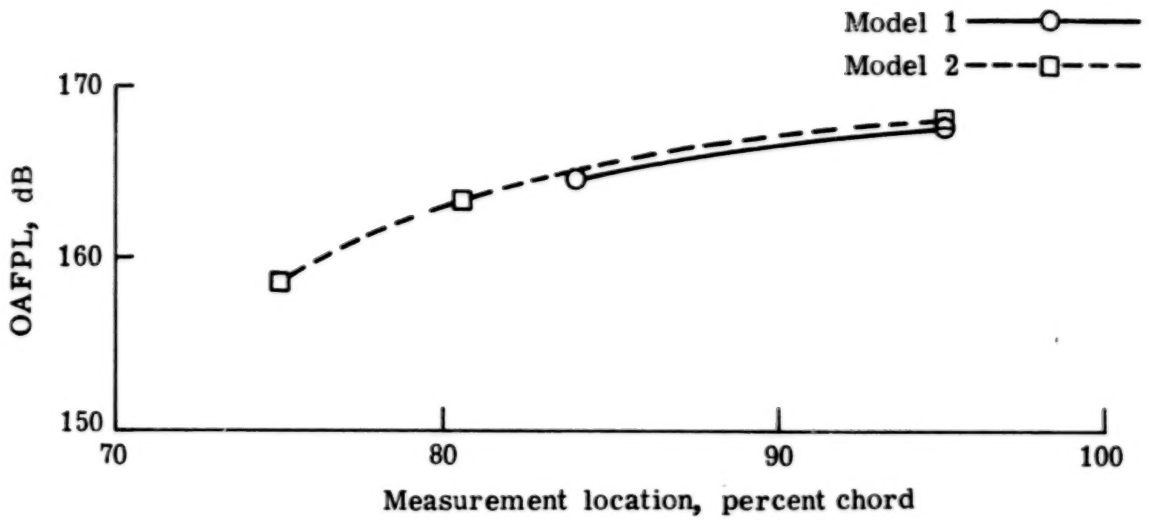

(a) OAFPL along jet center line. $\delta = 20^{o}$.

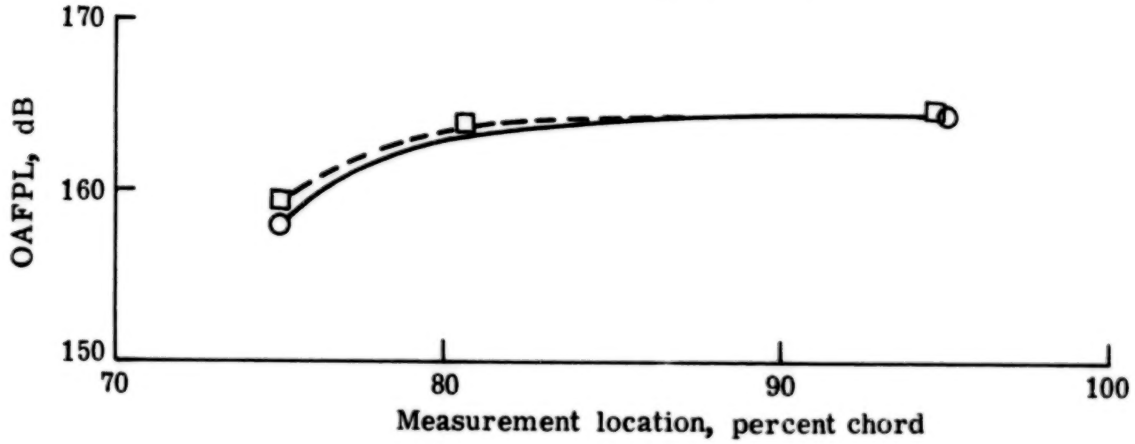

(b) OAFPL along jet center line. $\delta = 45^{o}$.

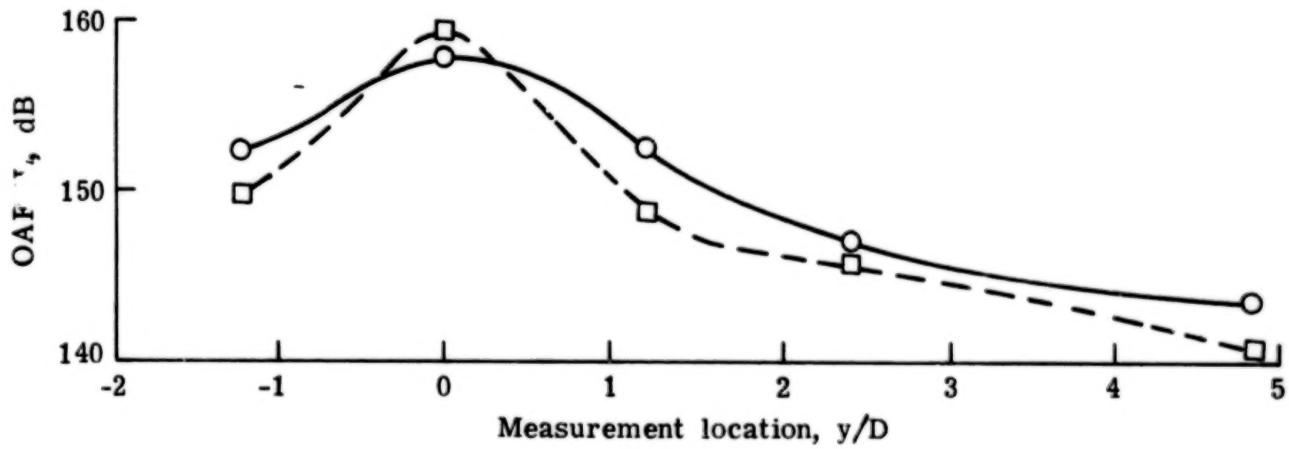

(c) OAFPL along 75 percent chord line of wing. $\delta = 45^{o}$.

Figure 3.- Comparison of overall fluctuating pressure levels (OAFPL) for models 1 and 2. $h/D = 0.3$; $\theta = 9^{o}$; jet exit at 65 percent c.

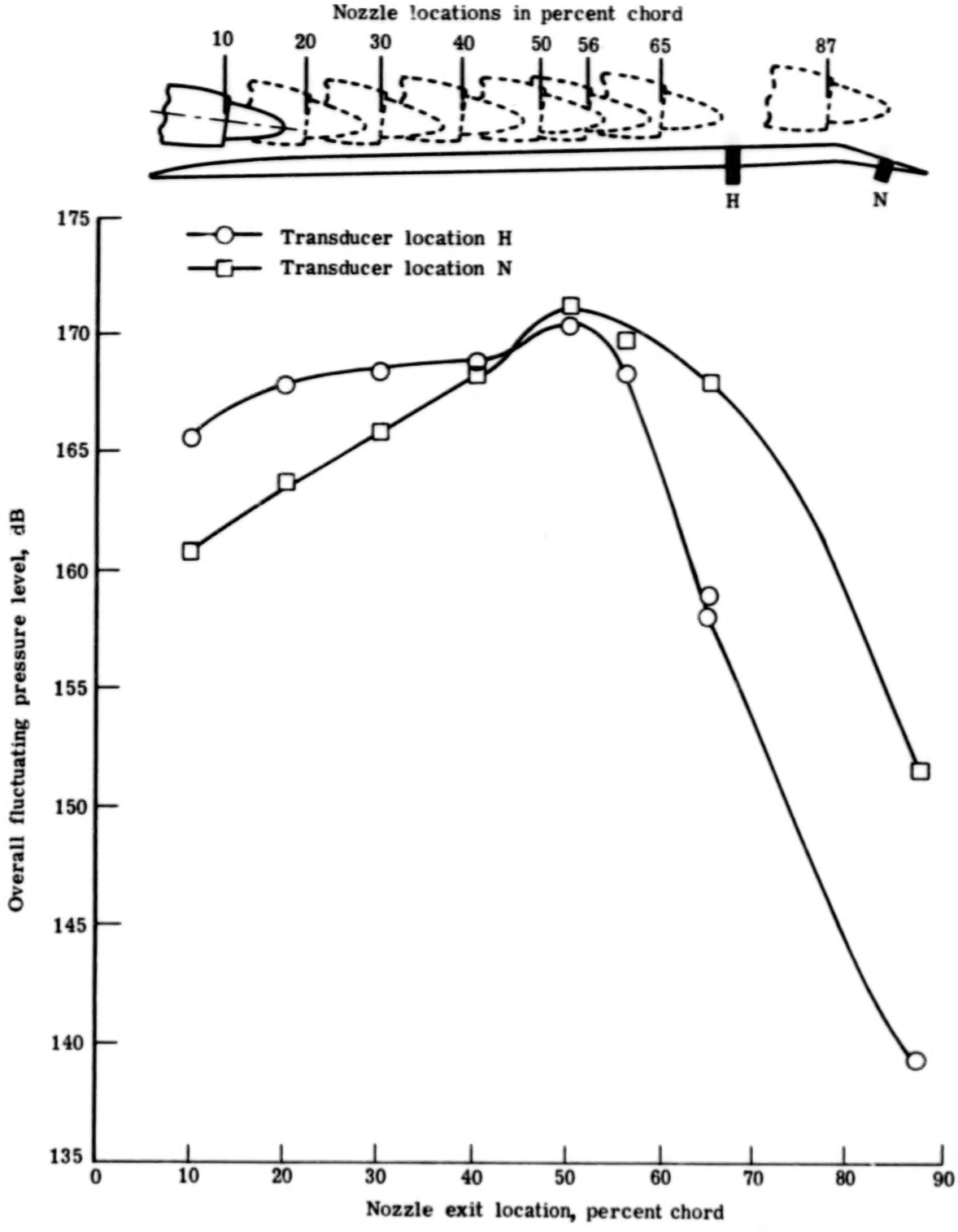

(a) OAFPL along jet center line.

Figure 4.- Effects of jet exit location on overall fluctuating pressure levels (OAFPL) measured on upper surface of wing. $h/D = 0.3$; $\theta = 9^{\circ}$; $\delta = 20^{\circ}$.

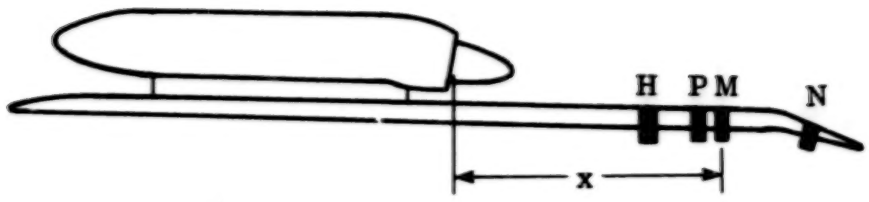

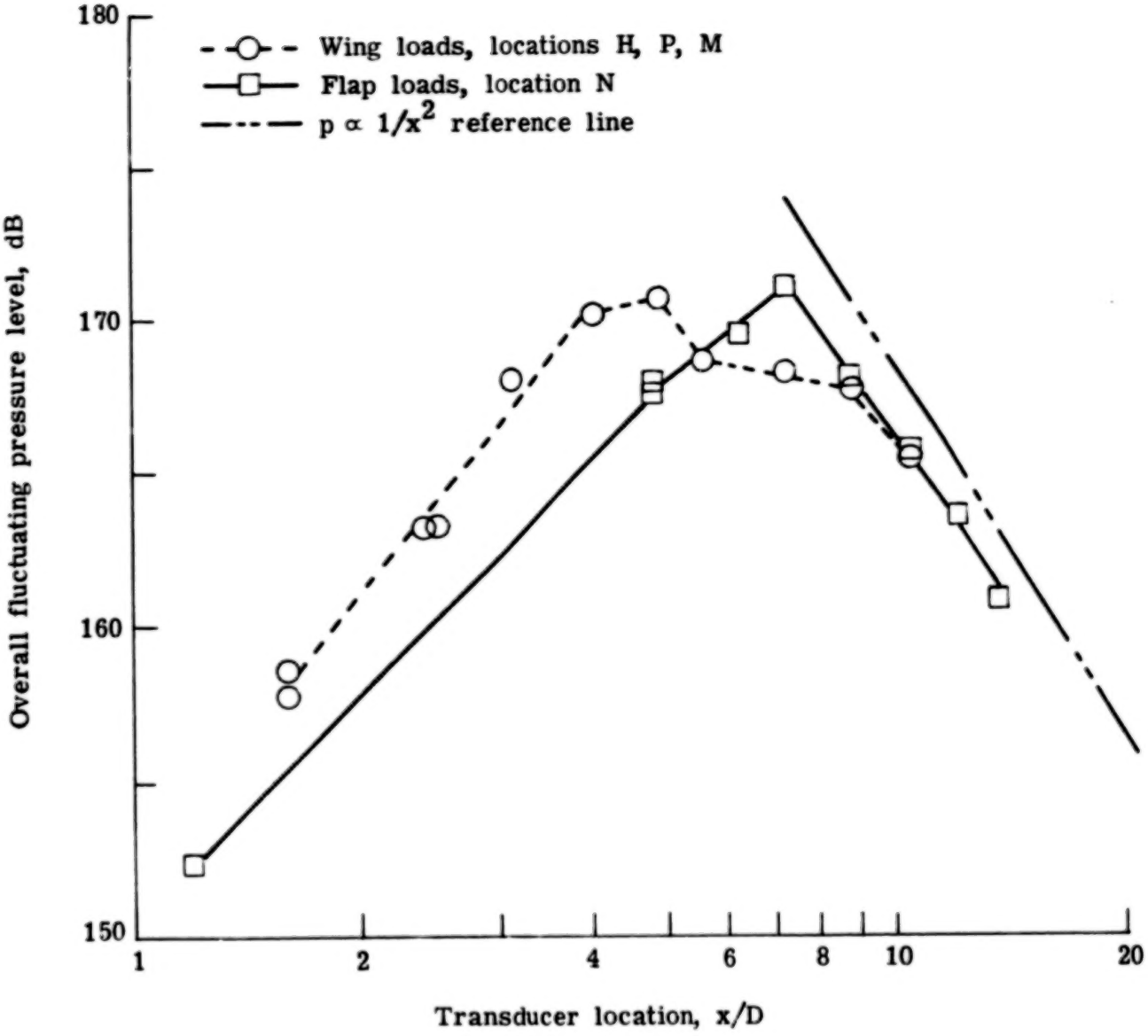

(b) Variation in center-line OAFPL with distance from nozzle.

Figure 4.- Continued.

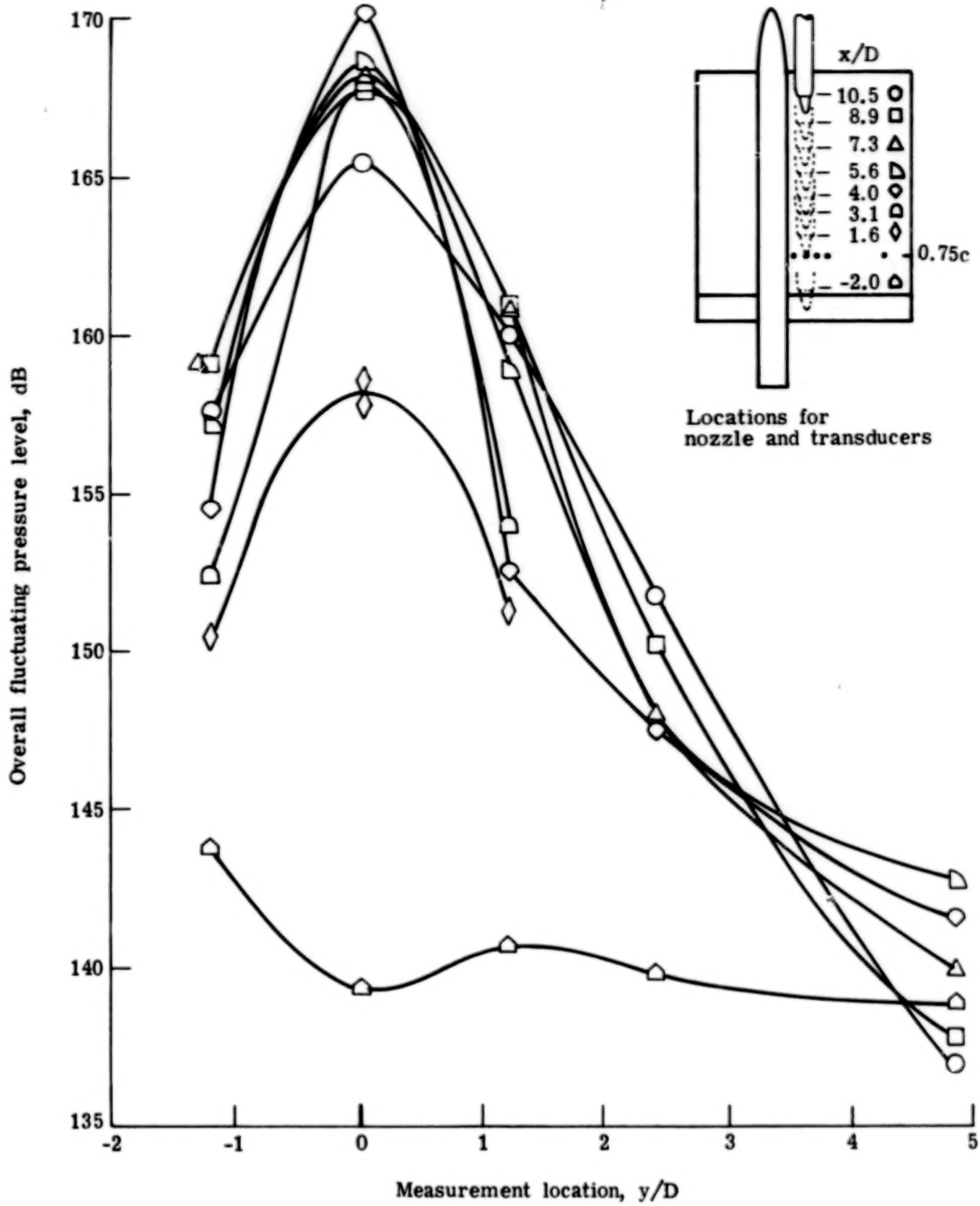

(c) OAFPL along 75 percent chord line of wing.

Figure 4.- Concluded.

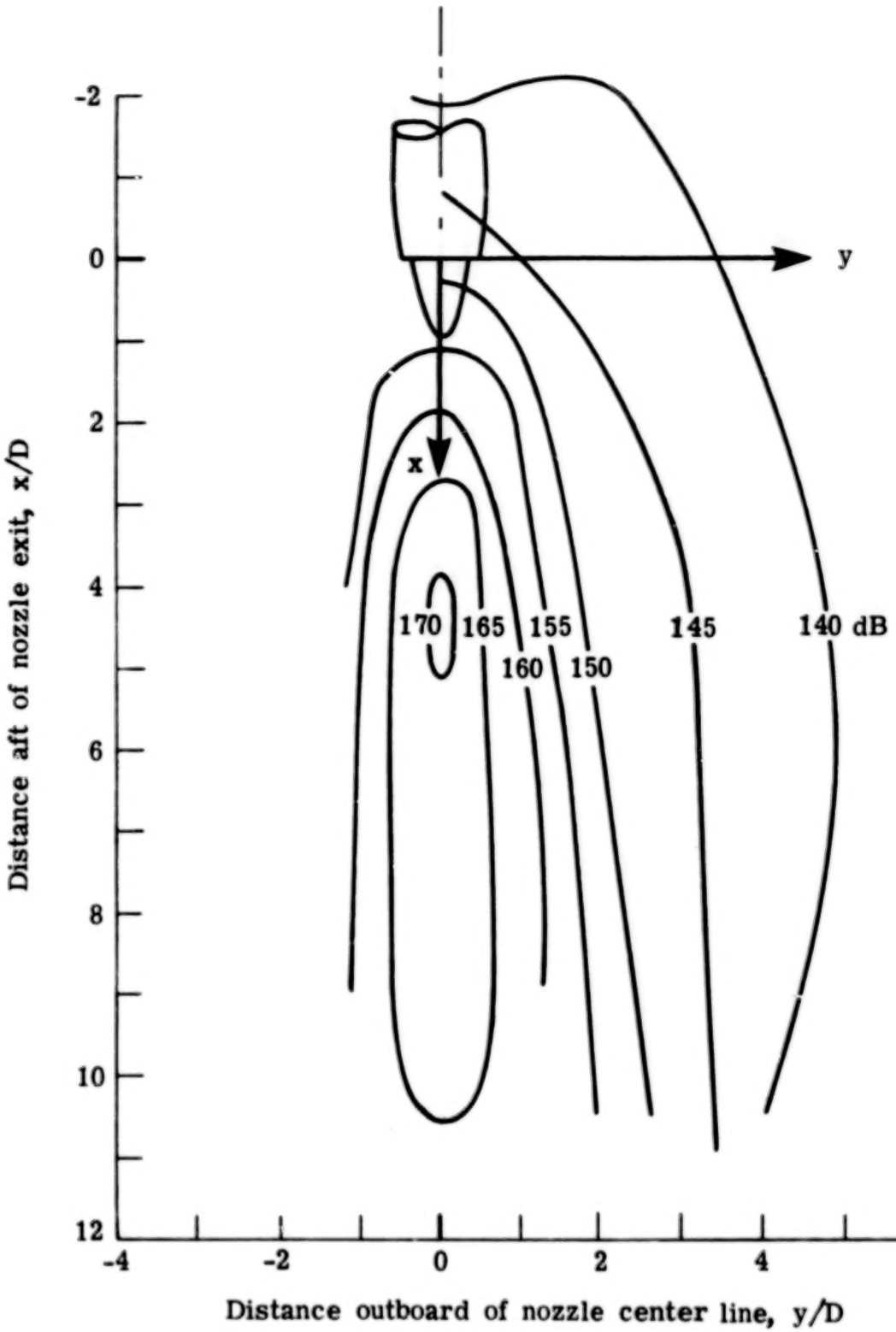

Figure 5.- Overall fluctuating pressure level (OAFPL) isobars on wing surface for h/D = 0.3 nozzle height and 9° impingement angle.

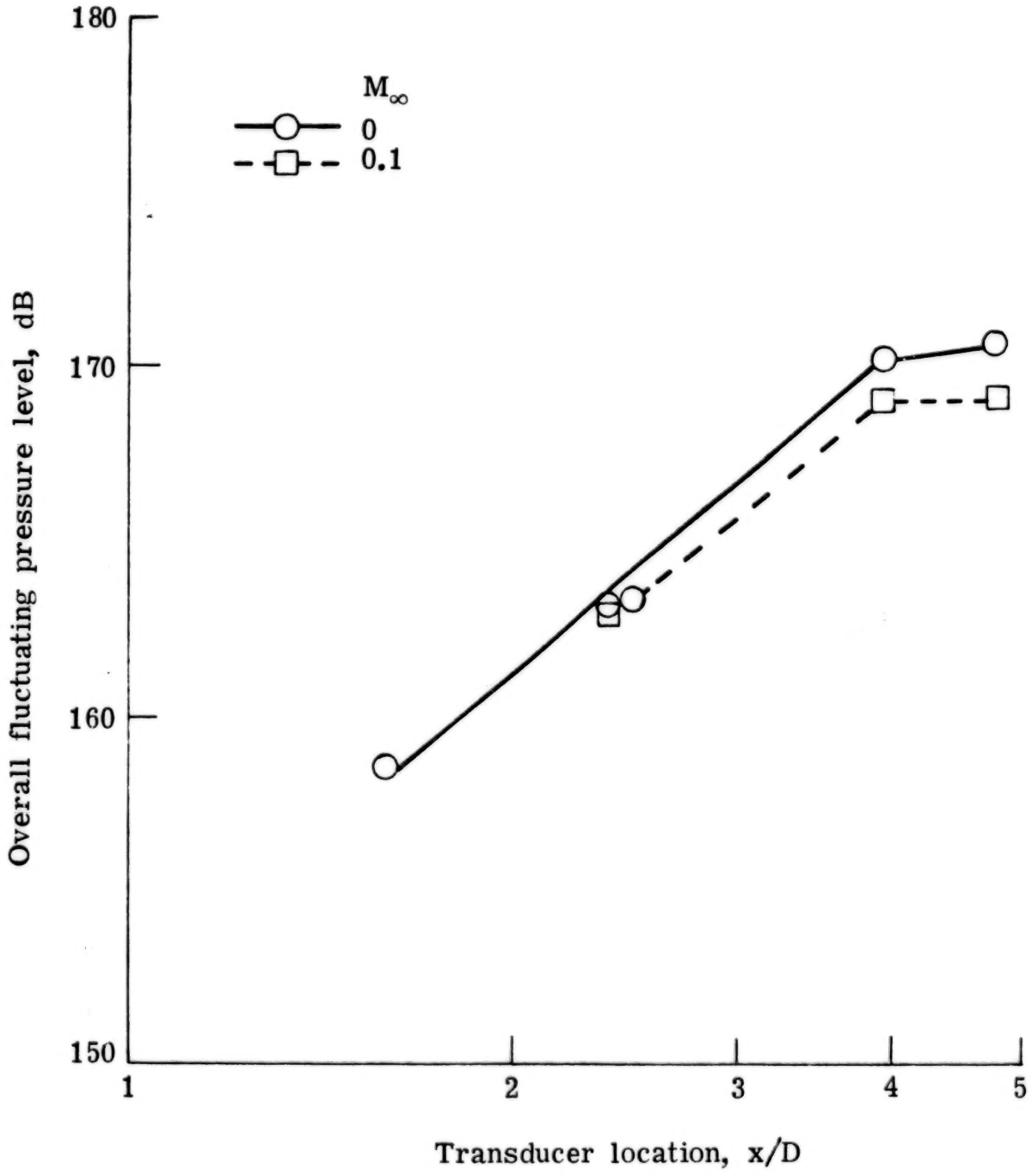

(a) Load along nozzle center line.

Figure 6.- Effect of airspeed on overall fluctuating pressure levels. h/D = 0.3; $\theta = 9^{o}$.

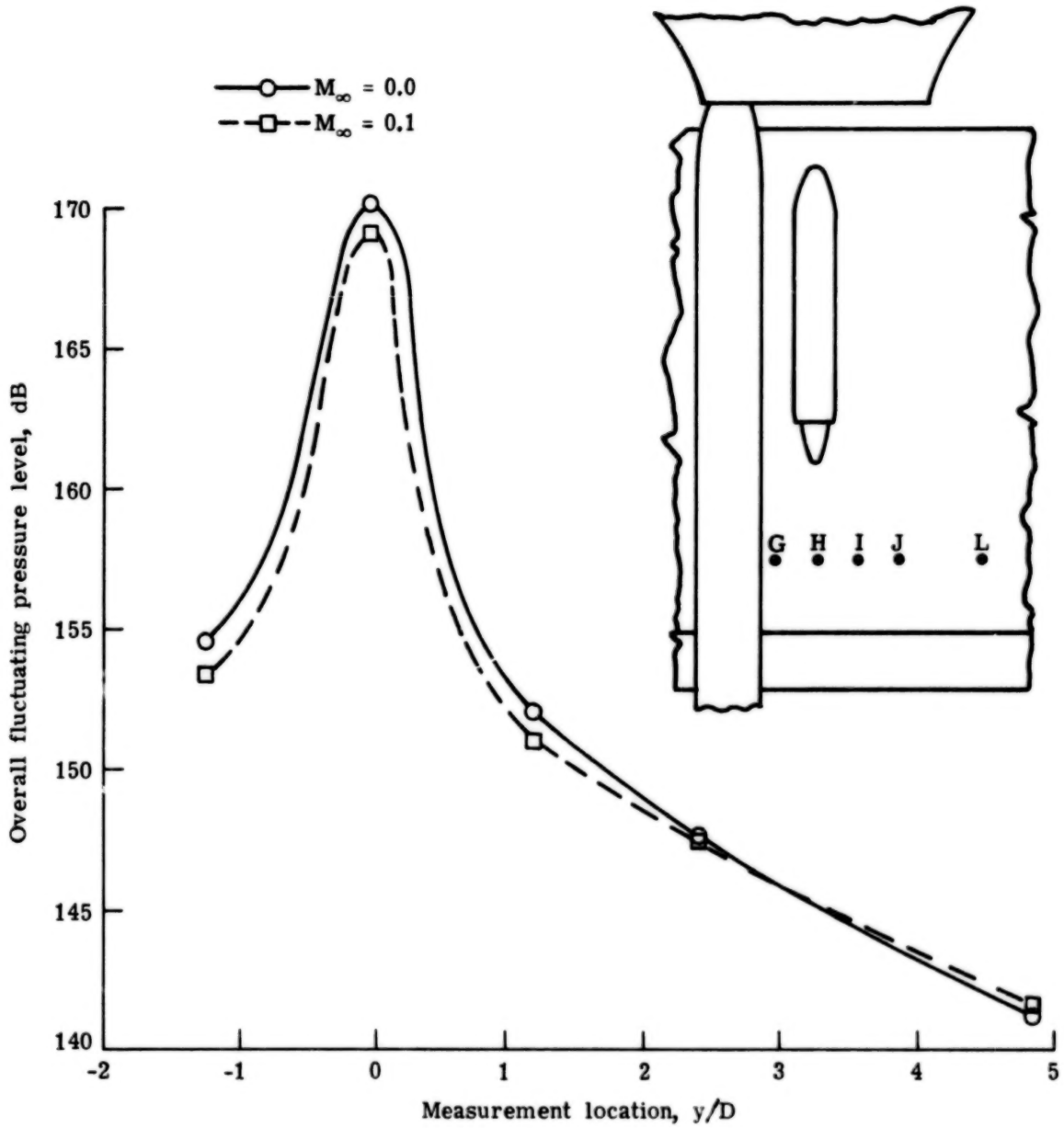

(b) Load along 75 percent chord line of wing. x/D = 4.

Figure 6.- Concluded.

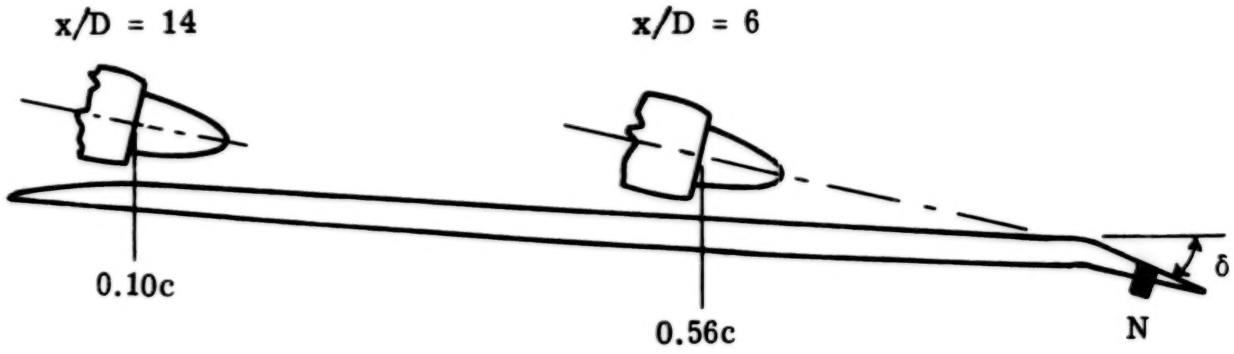

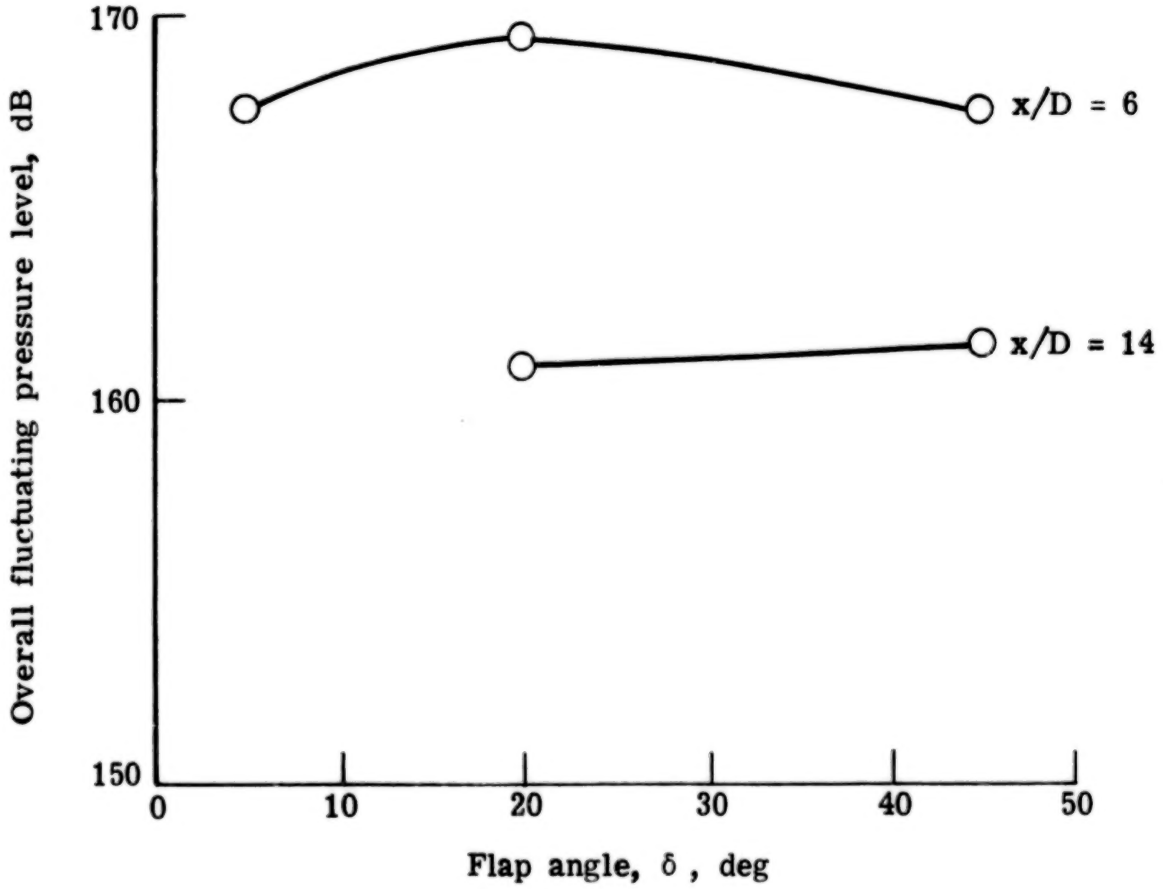

Figure 7.- Effect of flap deflection angle on flap loads.
h/D = 0.3; θ = 9°.

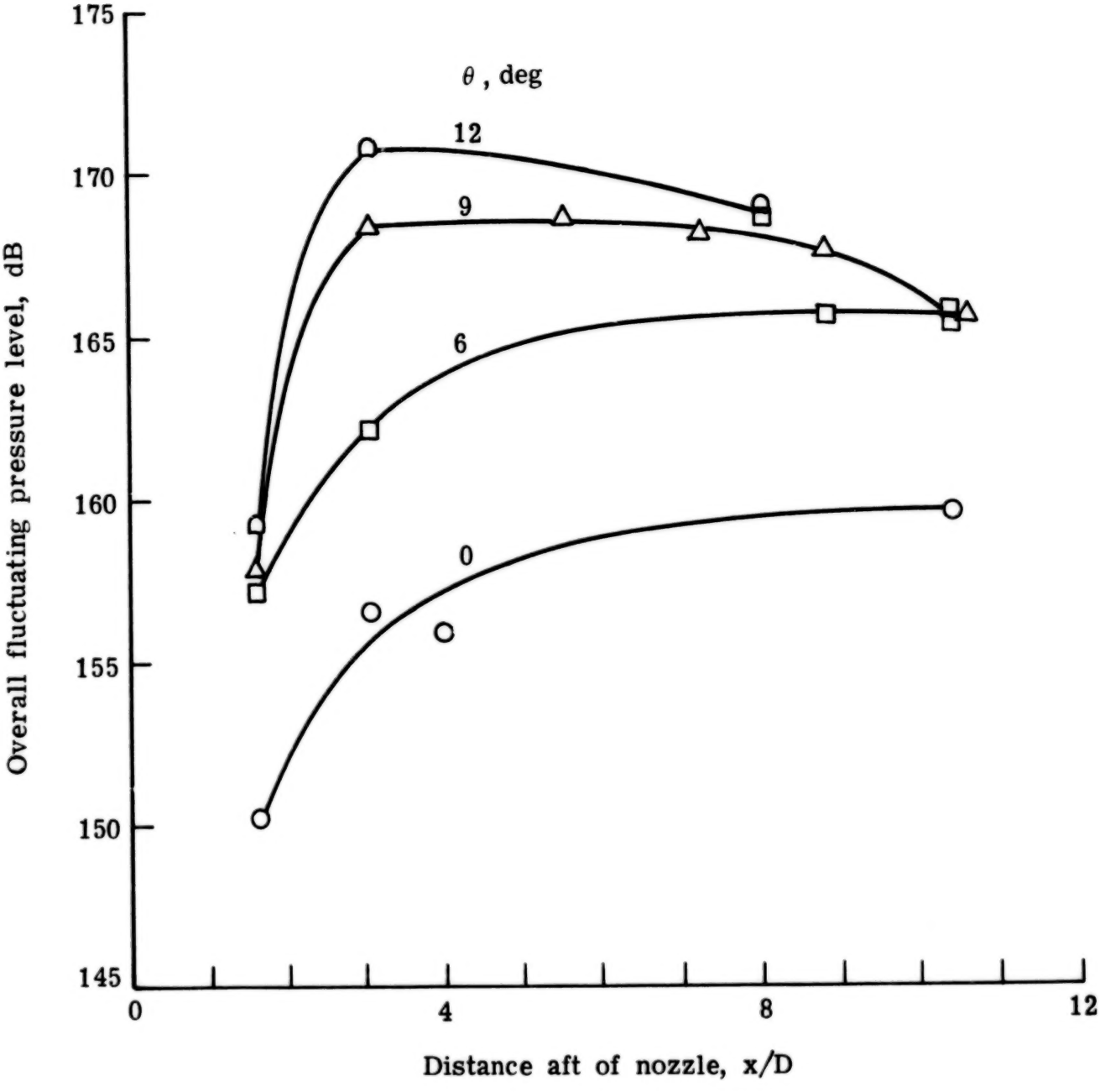

Figure 8.- Effect of jet impingement angle. h/D = 0.3; y/D = 0.

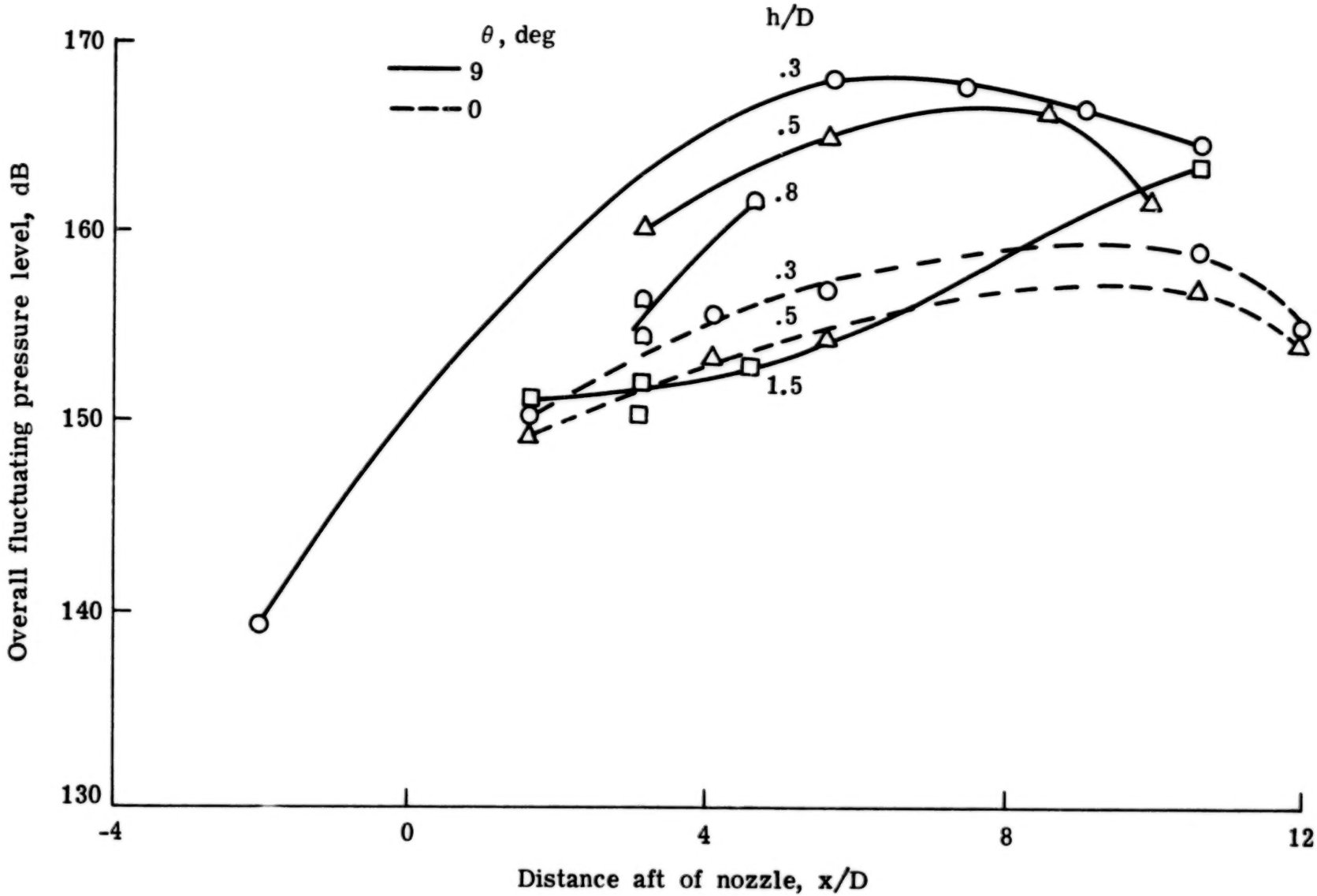

Figure 9.- Comparison of loads along center line for four nozzle heights.

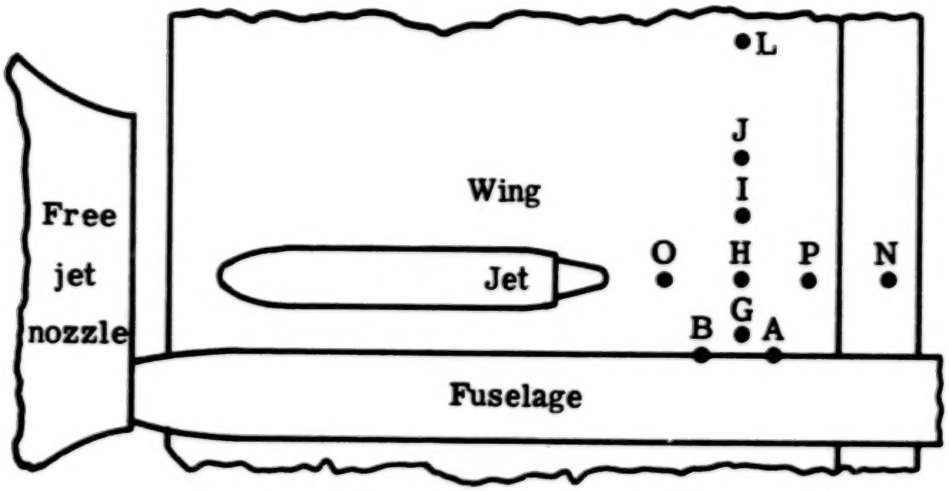

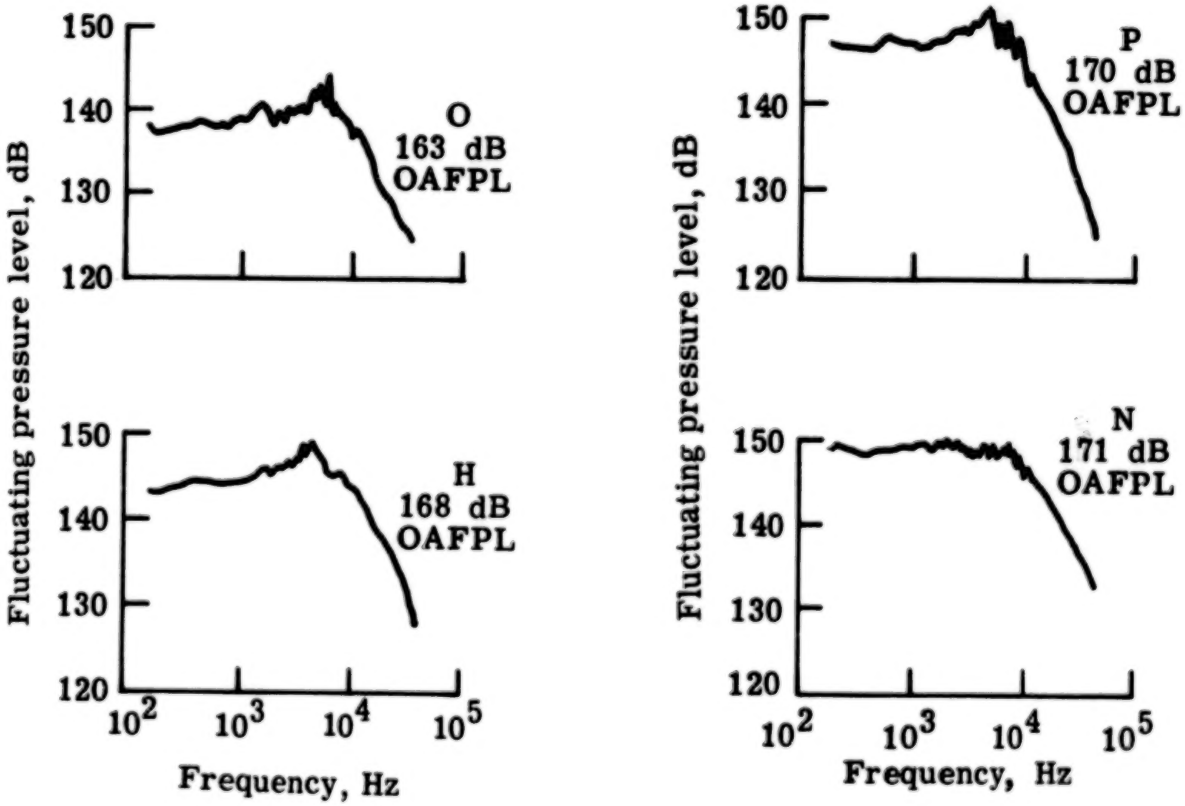

Figure 10.- Fluctuating pressure spectra (FPL) for 10 locations. Jet exit at 50 percent c; $\theta = 9^{o}$; h/D = 0.3; 100 Hz analysis bandwidth.

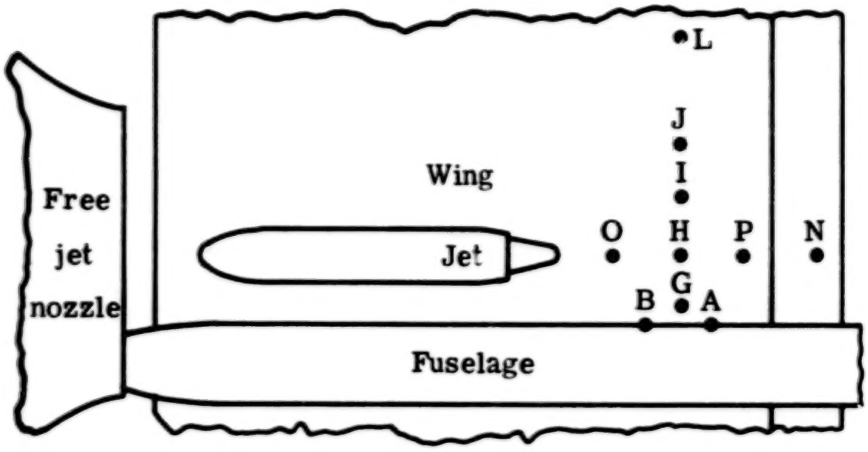

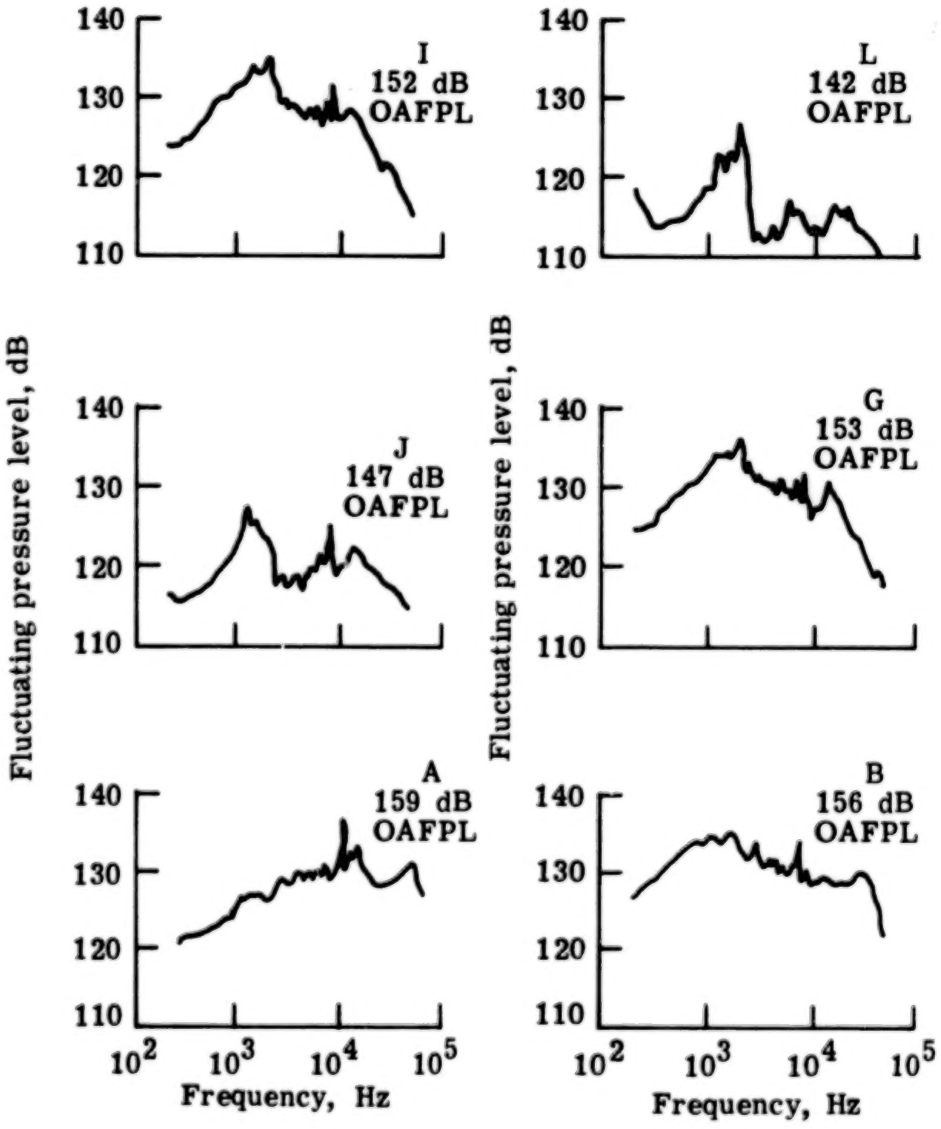

Figure 10.- Concluded.

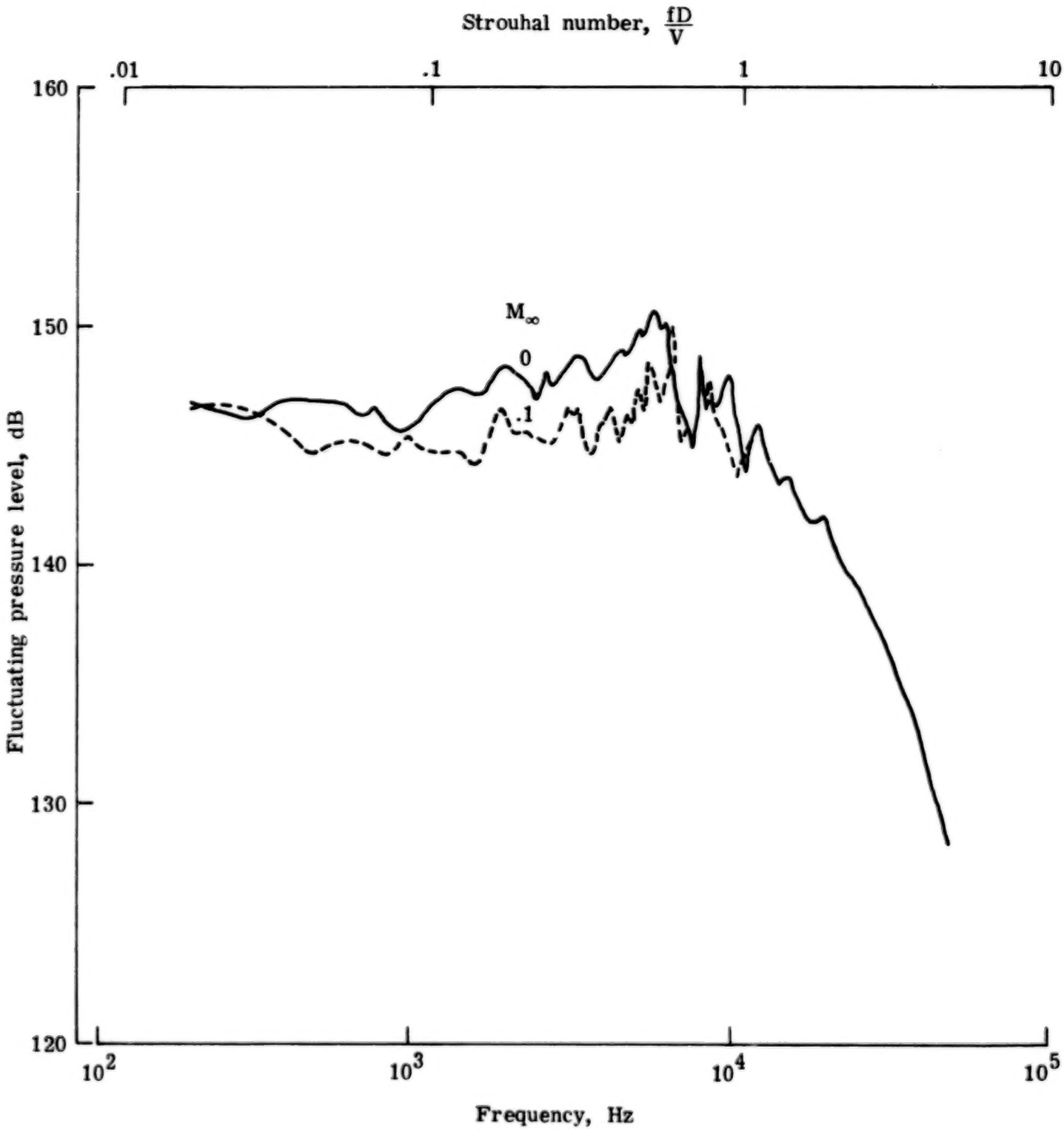

(a) Location forward of flap; x/D = 4.0; location H.

Figure 11.- Effect of airspeed on load spectra at nozzle center line. $\theta = 9^o$; $\delta = 20^o$; h/D = 0.3.

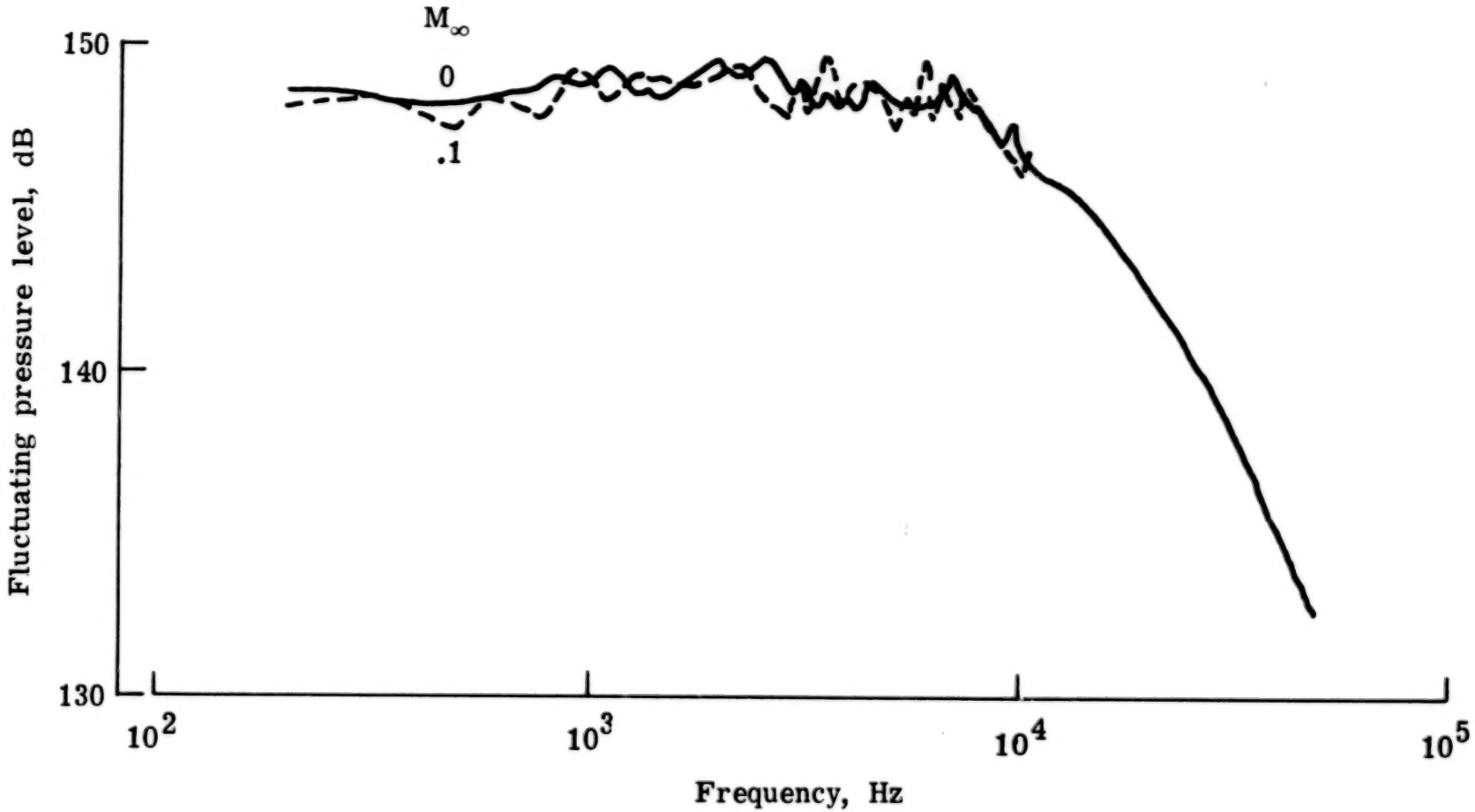

(b) Location on flap. x/D = 7.3.

Figure 11.- Concluded.

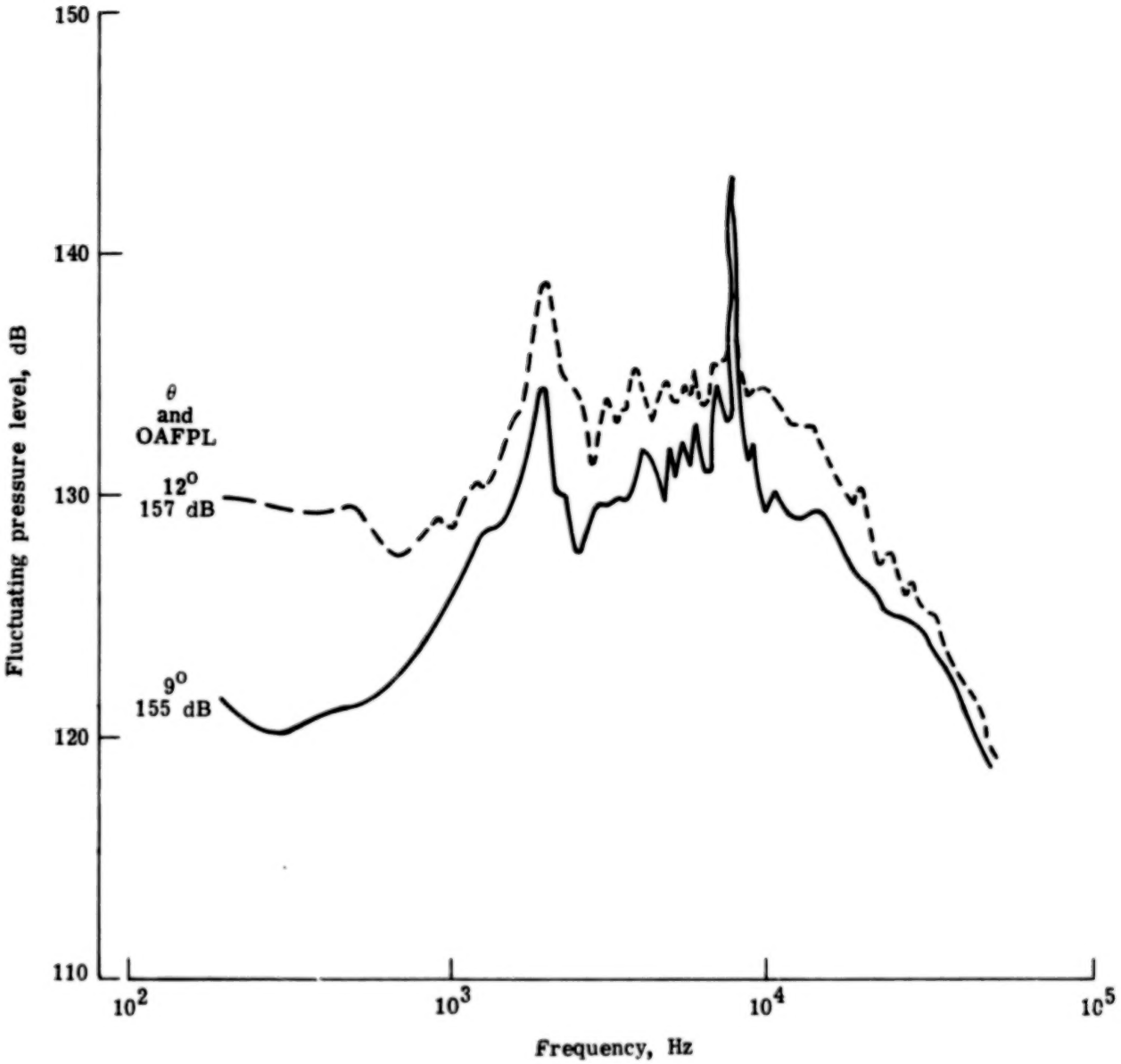

Figure 12.- Comparison of spectra for two impingement angles.
h/D = 0.3; x/D = 1.6.

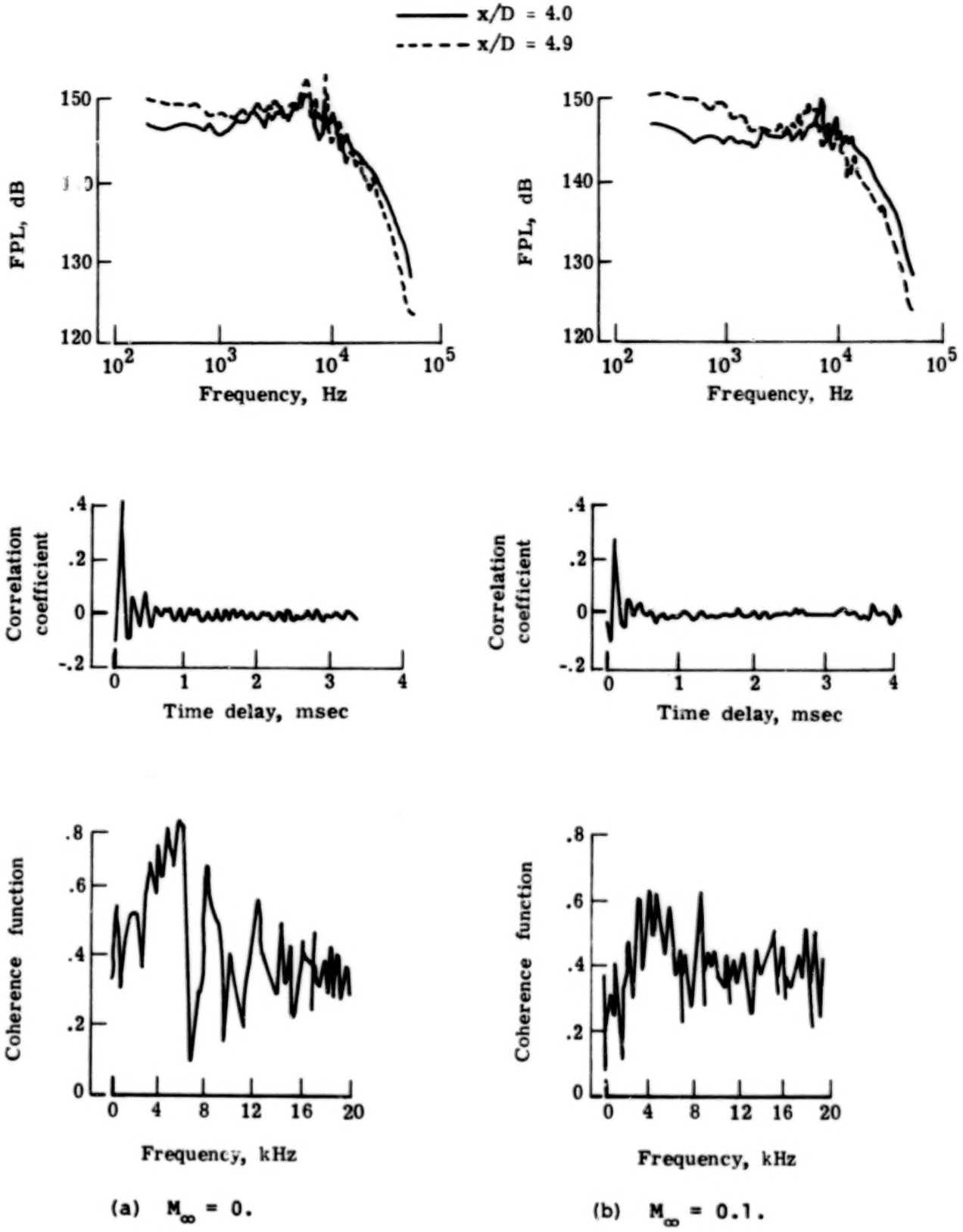

(a) $M_\infty = 0.$

(b) $M_\infty = 0.1.$

Figure 13.- Cross-correlation coefficients and coherence functions for two locations on the nozzle center line. h/D = 0.3; $\theta = 9^o$; locations H and M.

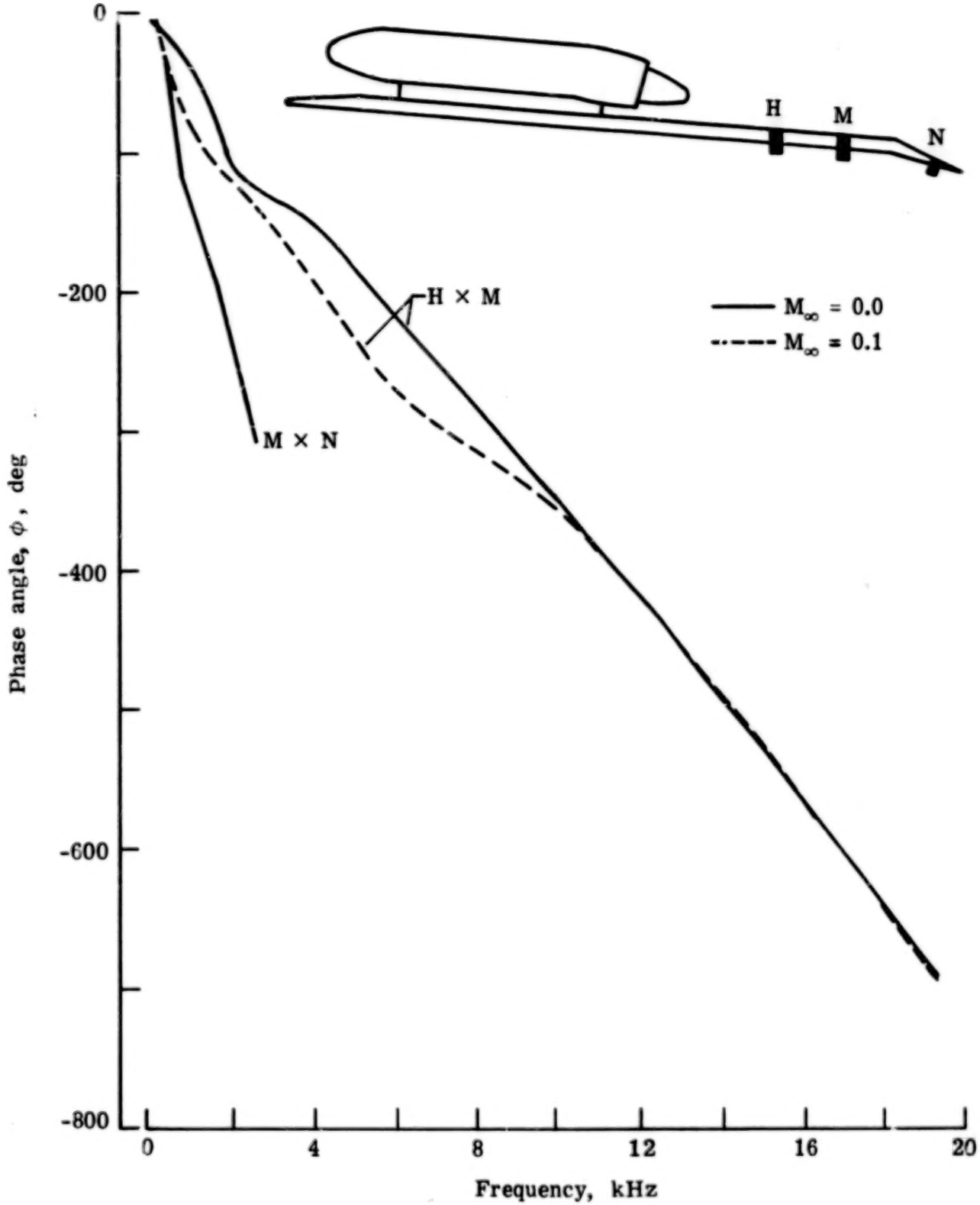

Figure 14.- Cross-spectral-density phase angle for two transducer pairs.

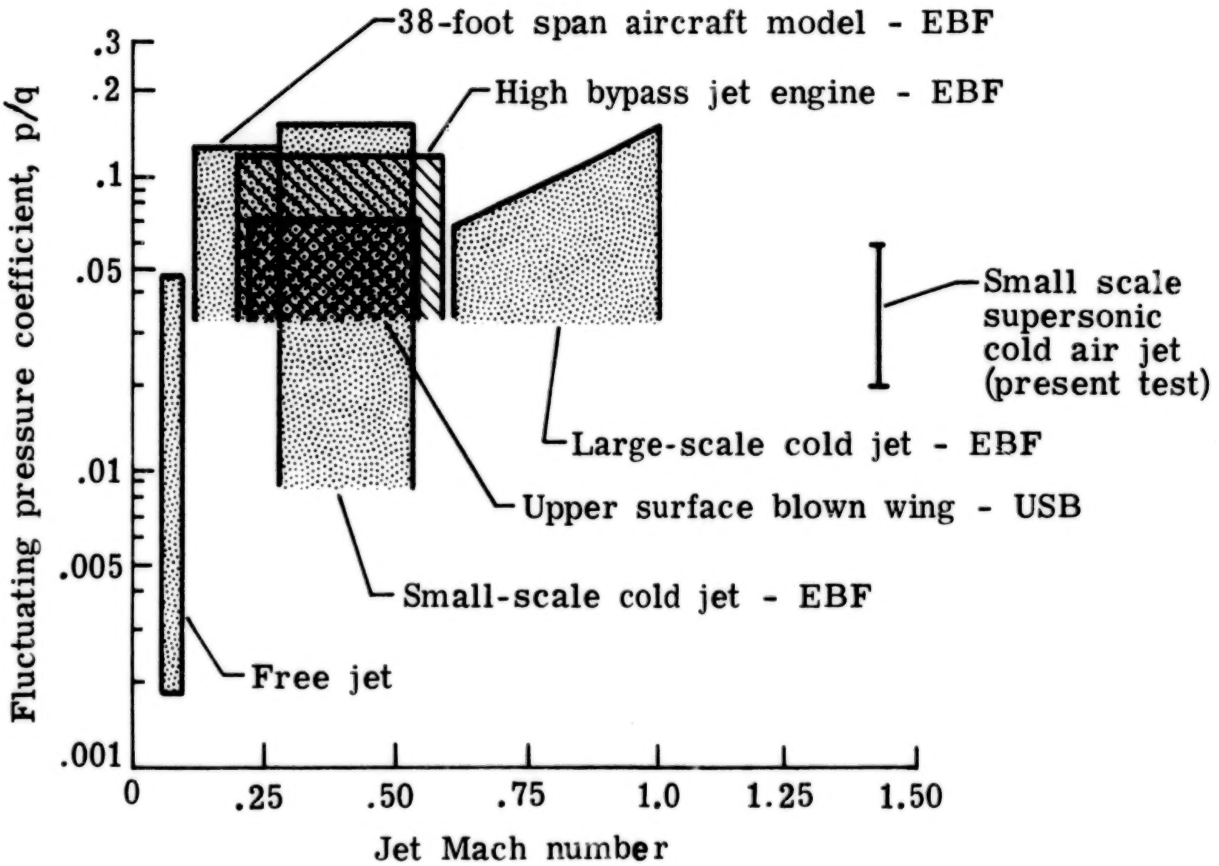

Figure 15.- Comparison of pressure coefficient for present test with subsonic coefficients from reference 13.

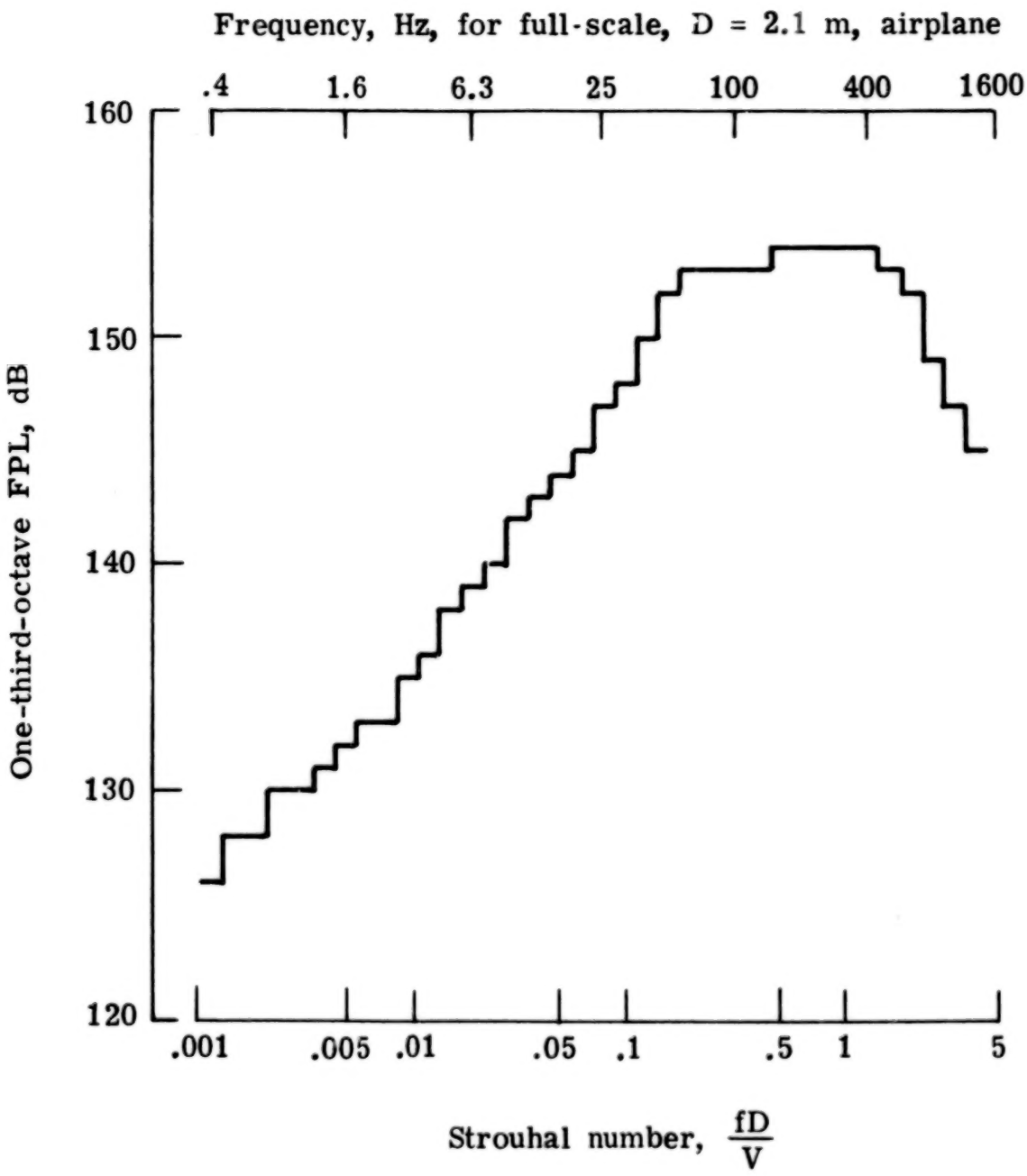

Figure 16.- Scaled one-third-octave spectrum for full-size airplane. $M_\infty = 0$; $y/D = 0$; $x/D = 8.9$.

1. Report No.	2. Government Accession No.	3. Recipient's Catalog No.
NASA TP-1366		

4. Title and Subtitle	5. Report Date
FLUCTUATING LOADS MEASURED ON AN OVER-THE-WING SUPERSONIC JET MODEL	January 1979
	6. Performing Organization Code
7. Author(s)	8. Performing Organization Report No.
Conrad M. Willis	L-12511
	10. Work Unit No.
9. Performing Organization Name and Address	505-09-23-11
NASA Langley Research Center Hampton, VA 23665	11. Contract or Grant No.
	13. Type of Report and Period Covered
12. Sponsoring Agency Name and Address	Technical Paper
National Aeronautics and Space Administration Washington, DC 20546	14. Sponsoring Agency Code

15. Supplementary Notes

16. Abstract

A test was conducted to measure fluctuating pressure loads on the wing and flap of an over-the-wing supersonic jet model. The model was tested statically and at a Mach number of 0.1 in a small free jet to simulate forward speed. Test parameters were impingement angle, nozzle height, and flap deflection. Load levels as high as 170 dB were measured at the center of the impingement region during static tests. Forward speed reduced the loading about 1 dB. Load level increased with increasing impingement angle and decreasing nozzle height above the wing. The effect of flap deflection was small. When scaled to full-size aircraft conditions, the maximum amplitude of the one-third-octave fluctuating pressure spectra was about 154 dB at about 160 Hz.

17. Key Words (Suggested by Author(s))	18. Distribution Statement
Acoustic loads Fluctuating pressures Upper surface blowing Supersonic jet	Unclassified - Unlimited Subject Category 71

19. Security Classif. (of this report)	20. Security Classif. (of this page)	21. No. of Pages	22. Price*
Unclassified	Unclassified	38	$4.50

* For sale by the National Technical Information Service, Springfield, Virginia 22161

NASA-Langley, 1979

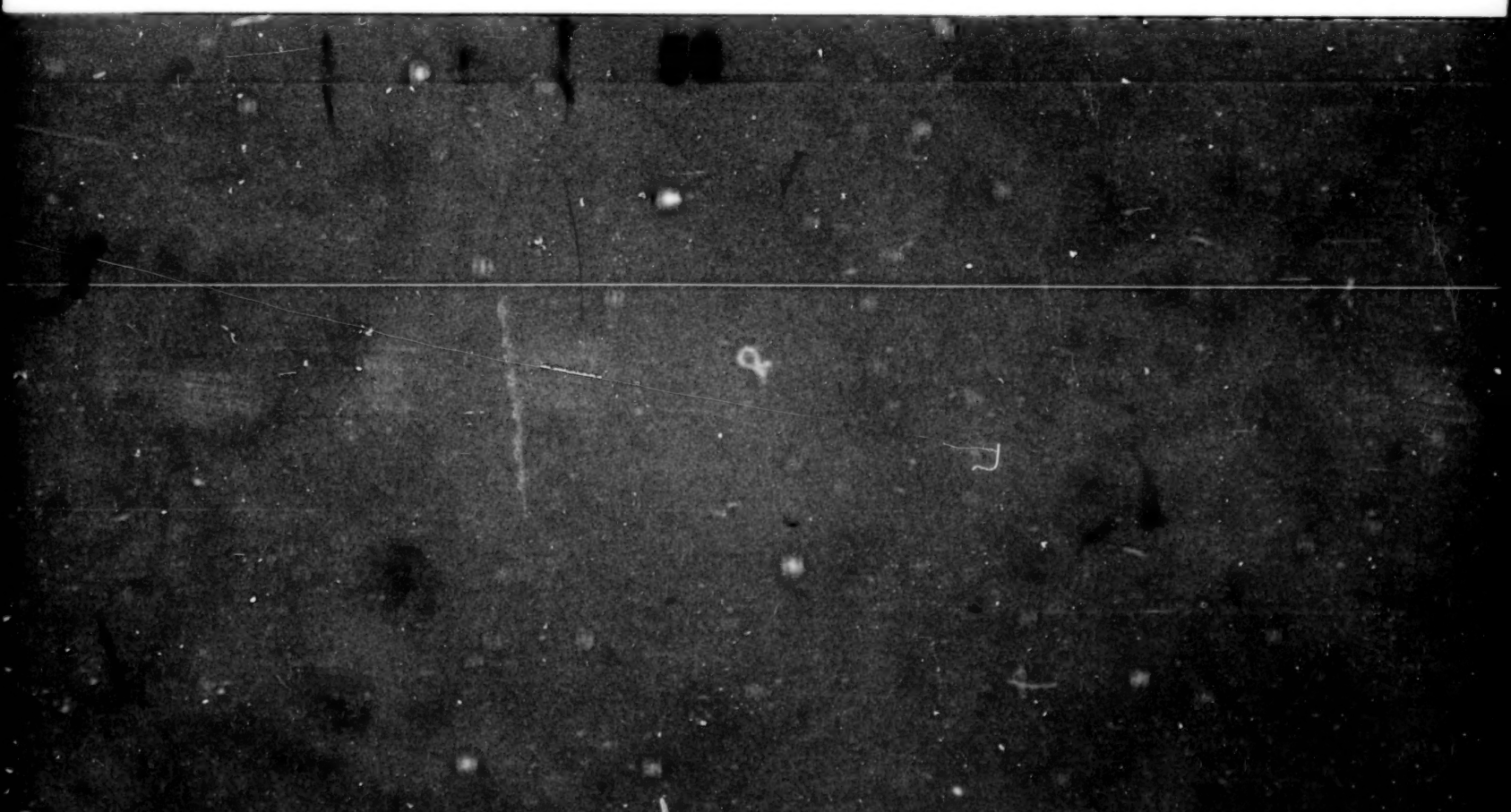

END

APR 30 1979